Journal of Inorganic Biochemistry 274 (2026) 113109

Contents lists available at ScienceDirect

Journal of Inorganic Biochemistry

journal homepage: www.elsevier.com/locate/jinorgbio

Influence of the intramolecular disulfide Cys46-Cys55 bridge on the interaction of human neuroglobin with SDS

Monica Caselli [a], Lorenzo Sebastianelli [b], Mirco Meglioli [a], Gianantonio Battistuzzi [a,*], Marco Borsari [a]

[a] Department of Chemical and Geological Sciences, University of Modena and Reggio Emilia, via Campi 103, 41125 Modena, Italy
[b] Department of Life Sciences, University of Modena and Reggio Emilia, via Campi 103, 41125 Modena, Italy

ARTICLE INFO

Keywords:
Neuroglobin
SDS
Cooperative effect
Disulfide bridge
Hydrogen peroxide
Oxidative degradation

ABSTRACT

Human neuroglobin (hNgb) is a globin involved in the protection of neurons and retinal cells which features an intramolecular disulfide bond between Cys46 and Cys55 under oxidative conditions. Here, conformational changes and oxidative degradation of hNgb wt and its C46AC55A mutant, lacking the disulfide bridge, were investigated in the presence of sodium dodecyl sulfate (SDS) by electronic absorption spectroscopy, intrinsic fluorescence emission and circular dichroism. Both proteins are found to undergo multiple SDS-induced conformational changes resulting in the formation of two non-native high spin species (HS1 and HS2). Moreover, increasing SDS concentration enhances the rate of heme breakdown by H_2O_2. Deletion of the Cys46-Cys55 disulfide bridge amplifies the conformational effect of SDS and appreciably increases heme oxidative degradation by H_2O_2.

1. Introduction

Human neuroglobin (hNgb) is a globin containing a single heme *b*, which is mainly expressed in different locations (cytosol, mitochondria, nuclei) of neurons of the central and peripheral nervous systems and in the retinal cells, although it is found in lower concentration in the gastrointestinal tract and in endocrine organs [1–7]. Contrary to hemoglobin and myoglobin, hNgb contains a six-coordinate heme *b*, whose axial coordination positions are occupied by the proximal and distal histidines (His96 and His64). Although the full understanding of the biochemical role of hNgb is still lacking, a neuroprotective function against hypoxia and ischemia was suggested [2,3], which is related to its ability i) to act as a ROS/RNS scavenger in the presence of increased levels of oxidative stress, ii) to reduce ROS production by interacting with the cytochrome *bc*1 complex, iii) to exert an antiapoptotic role, blocking the activation of the apoptotic pathway in H_2O_2-induced stress condition by preventing the cytosolic release of cytochrome *c* (Cyt-c) and iv) to modulate different intracellular signalling pathways involved in cell survival [8,9]. Therefore, hNgb appears to exert a cytoprotective role in the presence of excessive intracellular ROS concentration and to be involved in the response to internal and external oxidative stress [8,9].

Along with human cytoglobin (hCgb), human neuroglobin is the only member of the globin family featuring an intramolecular disulfide bond (connecting Cys46 and Cys55) in oxidizing conditions. Indeed, in vivo around 90 % of the hNgb molecules are in the deoxy-Fe(II) form without the disulfide bridge [10–13]. The latter is not observed in neuroglobin from other organisms [2,3] and plays a crucial role in controlling the structure of hNgb and the ability of the heme iron to bind small exogenous ligands (O_2, CO, NO) [14]. Indeed, upon cleavage of the Cys46-Cys55 disulfide bond, the loop connecting the helices C and D (CD loop formed by residues 36-59) [4,6,14–17] swaps from an α-helical structure to a β-turn followed by a short distorted β-strand (Fig. 1) [6,14,16]. This structural rearrangement results in a significant reorganization of the H-bonding network involving the heme propionates, without significantly affecting the heme cavity and the overall three-dimensional structure of the protein [14,16]. Indeed, the helix-to-strand rearrangement of the CD loop induced by the cleavage of Cys46-Cys55 disulfide bond moves Tyr44 close to the heme distal cavity (Fig. 1), where its sidechain interacts with that of the distal histidine and is involved in the distal H-bond network involving heme propionates, Glu60, Lys67 and a H_2O molecule [6,14,16]. Moreover, the cleavage of

* Corresponding author.
E-mail addresses: monica.caselli@unimore.it (M. Caselli), lorenzo.sebastianelli@unimore.it (L. Sebastianelli), mirco.meglioli@unimore.it (M. Meglioli), gianantonio.battistuzzi@unimore.it (G. Battistuzzi), marco.borsari@unimore.it (M. Borsari).

https://doi.org/10.1016/j.jinorgbio.2025.113109
Received 7 July 2025; Received in revised form 2 October 2025; Accepted 9 October 2025
Available online 10 October 2025

the disulfide bridge (or mutation of Cys46 and Cys55) strengthens the bond between the heme iron and the distal histidine, decreasing the affinity of hNgb for exogenous ligands, such as O_2, NO_2^- and CN^- [16,18–24] and enhancing its resistance to the oxidizing effect of H_2O_2 [25,26]. Therefore, the Cys46-Cys55 disulfide bridge [1–4,6,14–17,19–28] connects the ability of hNgb to bind exogeneous ligands to the redox state of the cell [3,18,20], thereby controlling the *in vivo* functionality of the protein. The third cysteine (Cys120) is far from the heme centre (Fig. 1).

Ionic surfactants are amphiphilic molecules which can induce protein denaturation through a complex multistep process based on a combination of electrostatic and hydrophobic interactions [29–31], which differs from that of chaotropic agents, such as urea and guanidinium chloride [32–36]. The interaction between proteins and surfactants has been widely studied using many different techniques, which provide complementary information [29,37–40]. These studies focused on the effects of surfactants on protein conformations [29,37]. A general accepted interpretation proposes that in the initial step the anionic surfactant binds, via electrostatic and hydrophobic interactions, to cationic side chains of amino acids and to nearby hydrophobic chains, respectively [37,41–44]. This first step, involving a specific binding and occurring at low surfactant/protein ratio, is followed by the formation of clusters of surfactant molecules that induce a progressive unfolding of the protein. For α-helical proteins, this process, has been suggested to involve three consecutive steps: a noncooperative binding, a cooperative binding, and finally the formation of "necklace and bead" structures in an unfolded protein [29].

Sodium dodecyl sulphate (SDS) is the most common anionic surfactant and it is widely used to probe protein structures [42,45–48]. The SDS-induced protein unfolding involves many intermediate states [30,31], whereas chaotropic agents induce the protein unfolding in few steps [32,35,49]. Below the critical micellar concentration (CMC), SDS is mainly present in the monomeric form, able to interact with proteins. Upon increasing concentration, SDS clusters are formed, which surround the proteins, thereby inducing the disruption of their tertiary and secondary structure. Above CMC, complexes among micelles of SDS and proteins are observed, and the latter are partially or completely unfolded [31]. The CMC value of SDS is about 7-8 mM in water, but decreases to 0.8-3 mM in phosphate buffer, depending on its concentration [37,50,51].

Absorption, CD and fluorescence spectroscopies are widely used to study the interaction between proteins and surfactants [52]. In particular, the fluorescence emission is very sensitive to the conformational changes of proteins, since the intrinsic fluorescence of proteins is due to the emission of aromatic amino acids tryptophan (Trp), tyrosine (Tyr), phenylalanine (Phe) and some enzymatic cofactors [53]. Tryptophans are usually the main source of fluorescence in proteins, because of the complete or partial fluorescence quenching of tyrosine and phenylalanine residues. The maximum of fluorescence emission of tryptophans is highly sensitive to their local environment, shifting from 351 nm for solvent-exposed residues to about 300 nm for those surrounded by a hydrophobic environment [54,55]. In heme proteins, the resonance energy transfer from tryptophans to the heme can be very efficient, since a representative Förster distance (R_0) for Trp to heme transfer is of 29 Å [56], and usually results in nearly completely quenched Trp emission [53]. hNgb possesses four Tyr and three Trp residues. Trp133, which belongs to the H helix, is the only one located in a hydrophobic cavity, whereas the other two tryptophans belong to helix A (Trp13) and helix H (Trp148), respectively (Fig. 1). The fluorescence properties of hNgb, described in this paper, are unusual compared to the other heme proteins, since the protein displays a well detectable emission and nanosecond fluorescence decay components.

The conformational changes in proteins can be followed by steady-state and time-resolved fluorescence techniques, namely by measurements of fluorescence intensity, lifetimes and anisotropy [57]. On the other hand, far-UV CD spectroscopy provides information on the secondary structure of the proteins, so that electronic absorption, emission and CD spectroscopy measurements constitute complementary essential tools for monitoring conformational changes in proteins [58–60].

Although the interaction of neuroglobin and cytoglobin with lipids was found to induce a shift of the equilibrium from the hexacoordinate to the pentacoordinate form of the heme [61], the influence of SDS on the conformation of hNgb has not been addressed so far. In principle, this interaction could induce extensive conformational perturbation and disrupt the distal Fe – His bond allowing the protein to acquire a pseudo-peroxidase reactivity. Therefore, understanding the changes in hNgb conformation and heme axial ligation upon interaction with increasing concentration of SDS would provide important insights about the factors influencing the overall stability of its 3D structure, which in turn influence its ability to act as a ROS scavenger in vivo [2,3]. Indeed, it is known that, in the presence of H_2O_2, hNgb undergoes to heme breakdown and dimerization/polymerization and that the latter process is triggered by tyrosyl radicals resulting from the oxidizing action of Compound I [25,26]. Although pseudo-peroxidase activity in heme proteins is crucial for some biological processes, it can become pathological when excessive or dysregulated, leading to oxidative stress and cellular damage. This activity, particularly when induced by conditions like inflammation or protein unfolding, can result in the formation of uncontrolled reactive oxygen species (ROS) that cause lipid peroxidation, DNA damage and protein modifications, including cross-linking and aggregation, contributing to various disease pathologies [62–66]. Since, the peroxidase activity of heme proteins can be significantly

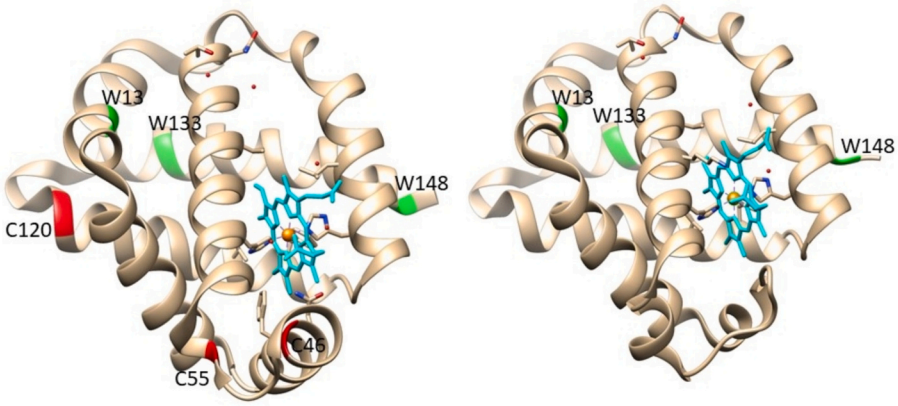

Fig. 1. Three-dimensional structure of wild type hNgb (left, pdb code 4mpm) and its C46G/C55A/C120S mutant lacking all cysteines (right, pdb code 1oj6). Heme (cyan), Trps (green) and Cys (red) are highlighted. Figures are drawn by Chimera package. (For interpretation of the references to colour in this figure legend, the reader is referred to the web version of this article.)

modified by conformational changes or unfolding it is interesting to verify to what extent the reactivity of hNgb with hydrogen peroxide is influenced by SDS-induced protein unfolding.

To clarify this issue, we analyzed the binding of SDS to hNgb wt and its C46AC55A mutant, lacking the disulfide bridge, using different spectroscopic techniques (UV − vis, CD and fluorescence emission). Since the mechanism of protein binding to anionic surfactants is significantly influenced by micellar structures, the study was carried out at concentrations lower, equal and higher than SDS CMC (about 2-3 mM in 50 mM phosphate buffer) [37,50,51]. This work aims at increasing our understanding of the effect of the Cys46-Cys55 disulfide bridge on the structural stability of hNgb, by elucidating the SDS-induced changes in the protein conformation, coordination and spin state of the heme iron and reactivity towards H_2O_2, both in the presence and in absence of the disulfide bond.

It turns out that both wt hNgb and its C46AC55A mutant undergo multiple SDS-induced conformational changes, resulting in the formation of two high spin conformers (HS1 and HS2). Moreover, the rate of heme breakdown by H_2O_2 increases with increasing SDS concentration. Therefore, deletion of the Cys46-Cys55 disulfide bridge amplifies the conformational effect of SDS and appreciably increases heme oxidative degradation by H_2O_2.

2. Materials and methods

2.1. Protein expression and purification

Wild-type human neuroglobin (hNgb) and its C46AC55A mutant were expressed in *E. coli* and purified as previously reported [1,25,26].

2.2. Measurements and instruments

UV–vis spectra were recorded with quartz cuvettes (1 cm path length) using a Varian Cary 100 Scan UV–vis spectrophotometer. The measurements were performed at 25 °C in 5–10 μM protein, 50 mM phosphate buffer plus 0.1 M NaCl (pH = 7.3) solutions, prepared immediately before use. The protein concentration was checked spectrophotometrically using $\varepsilon_{412} = 129{,}000\ M^{-1}\ cm^{-1}$ [21].

Fluorescence spectra were measured with a Horiba Fluoromax-4 spectrofluorometer using 0.4 × 1.0 cm quartz cuvettes (1 cm path length) and acquired with right-angle detection. The excitation and emission slit widths were set at 2 and 3 nm, respectively. The samples, whose absorbance at the excitation wavelength was less than 0.2, were excited at 280 or 295 nm. The fluorescence spectra were corrected for the instrumental spectral sensitivity, after the subtraction of the buffer signal. Fluorescence quantum yields (Φ_F) were determined at 25 °C upon excitation at 295 nm using L-tryptophan in phosphate buffer at pH = 7.3 as the standard ($\Phi_F = 0.13$ [67]). The absorbance at 295 nm was equal for the sample and the standard. Fluorescence lifetimes (τ_F) were measured with a Horiba FluoroMax4 time correlated single-photon counting equipment using, as the excitation source, a nano-LED emitting at 295 nm. Instrumental time resolution, after deconvolution, is 100 ps. Fluorescence decays were fit to a sum of exponentials using Horiba DAS6 software, considering that a fit with χ^2 value between 1.00 and 1.25 is adequate. Fluorescence emission anisotropy was measured using automated polarizers in FluoroMax4 fluorometer.

CD spectra were recorded with a Jasco J-810 spectropolarimeter using a quartz cuvette of 1 cm path length and samples containing 1.5 μM protein in 5 mM HEPES buffer plus 0.1 M NaCl at pH 7.3. In all cases, spectra were recorded 10 min after mixing. The CD spectra were measured in [θ] = mdeg. Since the UV–Vis spectra of hNgb wt and C46AC55A recorded in the presence of SDS at all the investigated concentrations do not change appreciably after about 5 min, all measurements were carried out after 10 min of incubation.

The effects of hydrogen peroxide on the electronic absorption spectra of wt and mutated hNgb were investigated using a Jasco V-570 spectrophotometer. All experiments were carried out at 25 °C with 3-5 μM protein solutions freshly prepared before use in 50 mM phosphate buffer plus 0.1 M NaCl, pH 7.3. Hydrogen peroxide was added to the above solution to a final concentration of 200 μM. Each addition of H_2O_2 was made 10 min after that of SDS to allow the protein spectrum to stabilize. All measurements were repeated at least three times on three independently prepared samples. Data are reported as the mean value obtained from the repeated experiments, and the associated error is the maximum deviation from the mean.

3. Results and discussion

3.1. UV–vis absorption spectra

The absorption spectra of hNgb wt and C46AC55A mutant are almost superimposable (Fig. 2), in agreement with the similarity of their heme pocket [14]. Both spectra are typical of six-coordinate ferric heme, featuring the Soret band at 413 nm and the Q bands at 532 and at 564 nm [1,25,26]. The absorptions by aromatic amino acids are observable in the range 250 - 300 nm (Fig. 2). In the absence of denaturants, hNgb features an equilibrium between a largely prevailing low-spin six-coordinate bis-His axially coordinated form and a high-spin species (either five-coordinate or six-coordinate with an axially bound water molecule) observed in very small amounts [68].

The changes induced by SDS in the electronic absorption spectra of the wt protein and the C46AC55A mutant are shown in Fig. 2: a decrease in intensity of the Soret and Q bands, along with a widening of the Soret band which becomes clearly asymmetrical, can be observed. In the range 0-10 mM SDS, the Soret band blue-shifts from 413 nm to 407 nm in wt protein and from 413 to 401 nm in the C46AC55A variant (Fig. S1), whereas the Q bands slightly red shift. In addition, in both cases a new band is observed at about 640 nm, whose intensity increases up to a SDS concentration of 4 mM and 2.5 mM for the wt protein and the C46AC55A mutant, respectively (Fig. 2B and D). At higher SDS concentrations this band is replaced by a new absorption at about 610 nm. For [SDS] ≤ 0.7 mM, two isosbestic points at 390/428 and 390/426 nm are observed for hNgb wt and the C46AC55A variant, respectively. Moreover, the double mutant shows a more marked decrease of the Soret and Q bands intensity compared to the native protein. The SDS-induced changes in the electronic spectra are summarized in Table S1.

A broad absorption band between 600 and 650 nm, which arises from the porphyrin-to-iron charge-transfer $a'_{2u}(\pi) \rightarrow e_g(d_\pi)$ transition (CT1) [69–72] is recognized as the specific marker of five- and six-coordinate high-spin Fe(III) heme proteins [61,69,70,72,73]. Therefore, the changes observed in the electronic spectra indicate that below the SDS critical micellar concentration (CMC), which in the experimental conditions employed for the measurements is about 2-3 mM [37,50,51], both proteins undergo a low-to-high spin transition, resulting in the formation of a high form (HS1), characterized by the CT1 at about 640 nm. This suggests that the surfactant monomers are the main responsible for the observed low-to-high spin transition. On the other hand, at SDS concentration higher than the CMC value (> 4 mM for wt protein, > 2.5 mM for the C46AC55A mutant) a second high spin species develops (HS2, whose CT1 is at about 610 nm), indicating that formation of SDS micellar structures heavily impacts on the environment of the high-spin heme.

The effects of increasing SDS concentration on wavelength and absorbance of the Soret band of the low and high spin species (λ_{Soret} = 413 and 401 nm, respectively, Figs. S1 and S2 A, B) clearly indicate that the electronic properties of the heme group of hNgb wt and C46AC55A undergo to relevant changes, which are remarkably different for the two proteins. The λ_{Soret} of both proteins is almost unchanged up to [SDS] = 1 mM and blue shifts in the presence of higher SDS concentration (Fig. S1). For hNgb wt, λ_{Soret} decreases almost linearly up to [SDS] = 10 mM to a final value of 407 nm, whereas that of the mutant sharply decreases to

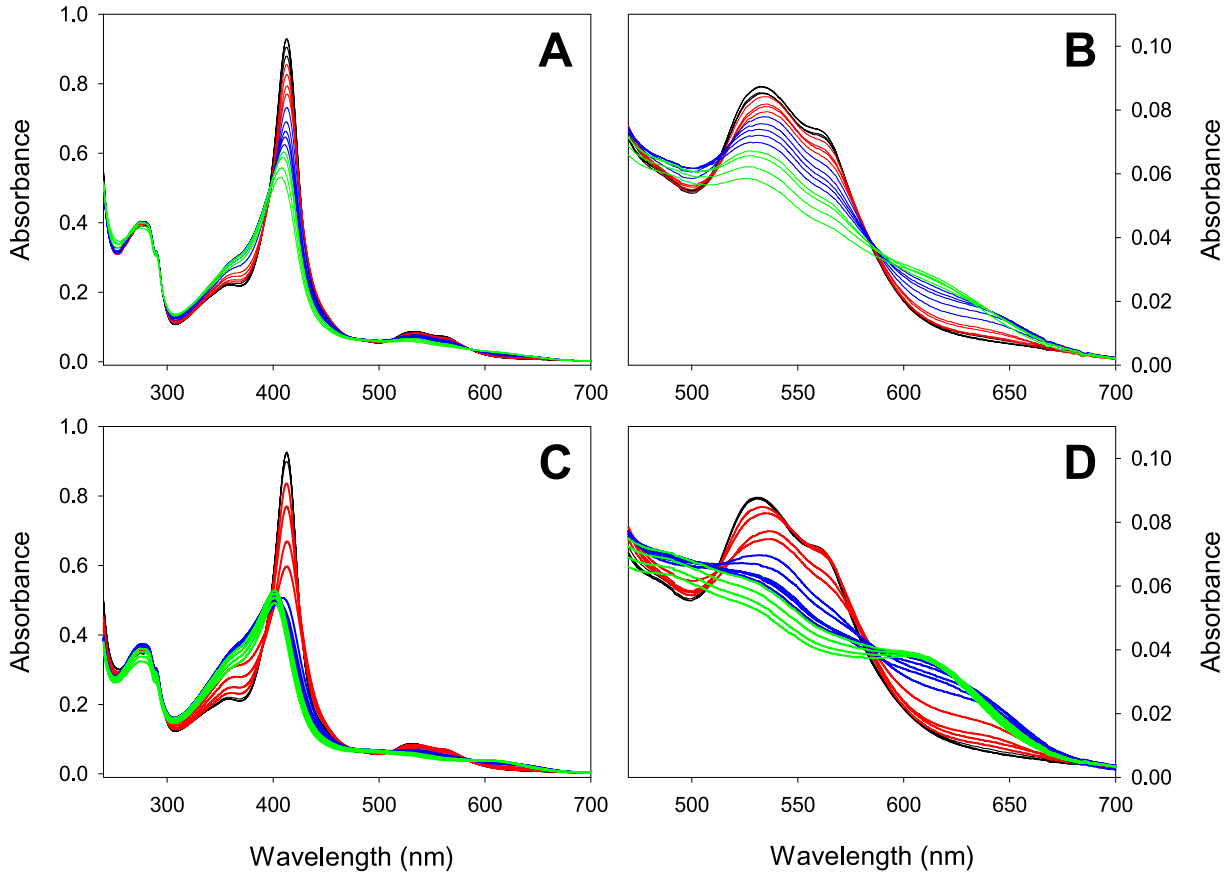

Fig. 2. Absorption spectra of hNgb wt (A, B) and its C46AC55A mutant (C, D) in the presence of increasing SDS concentrations: 0 ≤ [SDS] ≤ 0.3 mM, black; 0.4 ≤ [SDS] ≤ 1.0 mM, red; 1.5 ≤ [SDS] ≤ 4.0 mM, blue; 5.0 ≤ [SDS] ≤ 10.0 mM, green. 50 mM phosphate buffer plus 0.1 M NaCl solution (pH = 7.3), T = 25 °C. (For interpretation of the references to colour in this figure legend, the reader is referred to the web version of this article.)

401 nm between 1 mM and 2.5 mM SDS and is unchanged in the presence of higher SDS concentrations (Fig. S1). The absorbance at 413 nm of hNgb wt decreases for [SDS] ≥ 0.2 mM with progressively decreasing slopes, corresponding to 0.2 mM ≤ [SDS] ≤ 0.75 mM, 0.75 mM ≤ [SDS] ≤ 3.0 mM and [SDS] ≥ 3.0 mM, whereas that of the C46AC55A mutant undergoes a greater and sharper decrease between 0.3 mM and 2 mM SDS and further decreases at SDS concentrations higher than 4 mM (Fig. S2 A). The absorbance at 401 nm of the wt protein sharply drops up to [SDS] = 1 mM and a further reduction is observed for [SDS] ≥ 4 mM, while that of the C46AC55A mutant dramatically decreases up to [SDS] = 1 mM, increases up to [SDS] = 5 mM and further decreases at higher SDS concentrations (Fig. S2 B).

Fig. 3 A and B show that changes in absorbance of the CT1 bands (at 640 nm and 610 nm) of the two high-spin conformers HS1 and HS2 that form with increasing SDS concentration are far greater for the C46AC55A mutant than for the wt protein. In particular, the absorbance at 640 nm of the latter markedly grows up to [SDS] = 3 mM, slightly increases up to [SDS] = 8 m and decreases at [SDS] = 10 mM, whereas the absorbance at 640 nm of the C46AC55A mutant increases up to [SDS] = 2 mM and decreases above [SDS] = 4 mM. The absorbance at 610 nm of both proteins increases with increasing SDS concentration, showing a clear inflection point at about [SDS] = 4 mM for the wt protein and at [SDS] = 2 mM for the C46AC55A mutant. The above results indicate that formation of the high spin species HS1 and HS2 occurs in the presence of lower SDS concentrations in hNgb C46AC55A compared to the wt protein. Hence, it appears that the former has a higher affinity for SDS monomers and is more prone to conformational changes compared to the latter.

Analysis of the 2nd derivative absorption spectra provides further insight into the effect of increasing SDS concentrations on the electronic properties of the heme group in both proteins (Figs. 3 C, D and Fig. 4) [74–76]. The troughs corresponding to the bands of the low spin form of the C46AC55A mutant (Figs. 4 C, D) observed in the absence of SDS (LS1) undergo to a 1-3 nm red shift and become progressively shallower for 0.3 mM ≤ [SDS] ≤ 2.0 mM, disappearing at [SDS] = 1.7 mM. A similar decrease is observed for the trough associated with the Soret band. In the same interval, a new trough appears at 640 nm, whose depth increases with increasing SDS concentration. For [SDS] ≥ 2 mM, new minima at 403, 490 and 532 nm are observed, whose depth progressively increases, and the minimum at 640 nm is progressively replaced by a new broad trough centered at 610 nm (Figs. 4 C, D).

The absorption bands observed in the spectral region around 550 nm are generally referred to as α and β bands, whereas in the spectroscopic literature they indicated as Q_0 and Q_v bands [77–79]. The latter, in particular, results from the superpositions of a significant number of overlapping vibronic bands assignable to the excitation of the first vibrational state of mostly A_{2g}-modes in the electronic Q-state, which are subject to band splitting due to the low symmetry of the protein environment [77–79]. Therefore, the peak positions in the absorption and the second derivative spectrum are affected by changes of the out-of-plane deformations of the heme resulting from multiple heme-protein interactions, which alter its ground and excited states [77–79]. Hence, the redshift of the troughs corresponding to the absorption bands of the native low-spin species (LS1) suggests that alterations in the out-of-plane deformations of the low-spin heme are occurring up to 1 mM SDS, whereas the appearance of the trough corresponding to the CT band around 640 nm and the progressive increases of its intensity indicates that the high spin form HS1 is formed for 0.5 mM ≤ [SDS] ≤ 2.0 mM (Fig. 3 D). Above 1.5 mM [SDS], no low spin species is present and for [SDS] ≥ 1.7 mM the HS1 form converts into the high-spin species

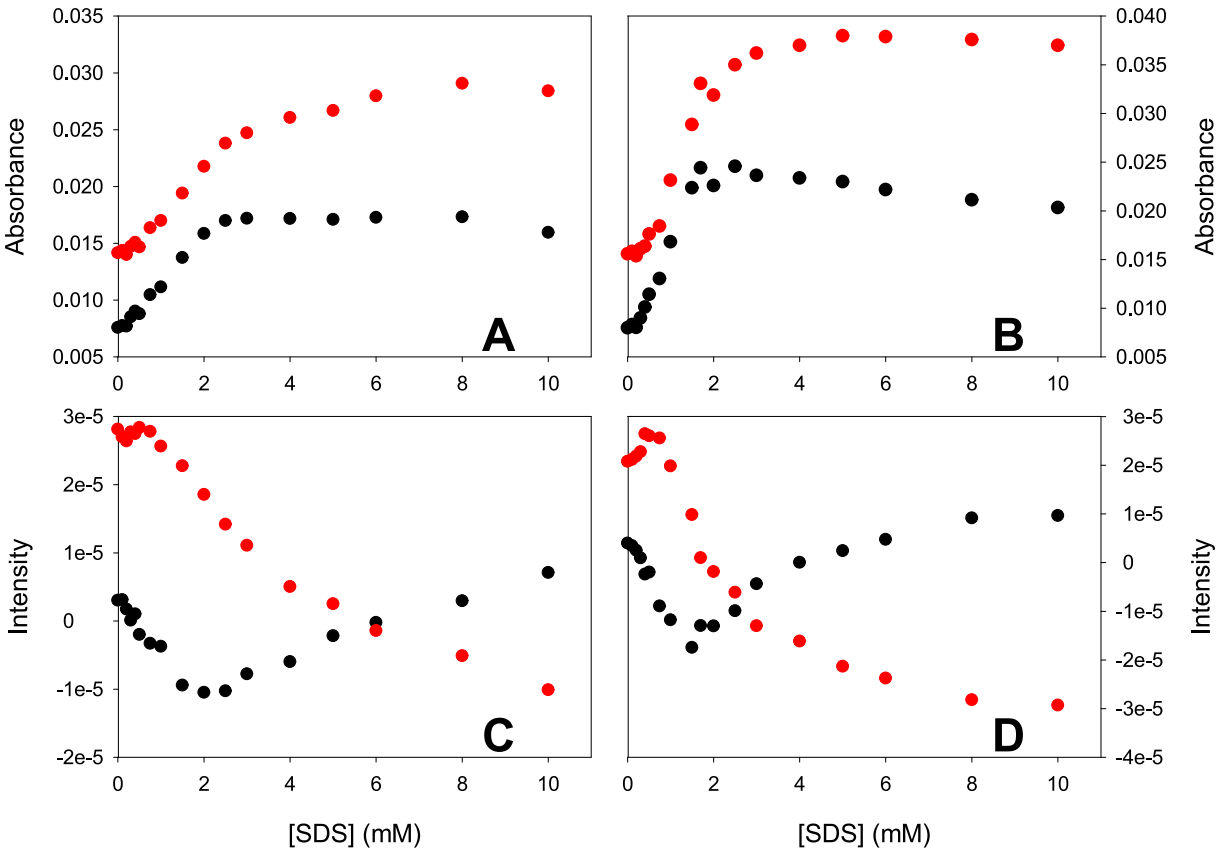

Fig. 3. Changes in the absorbance and in the intensity of 2nd derivative electronic absorption spectra of hNgb wt (A, C) and its C46AC55A mutant (B, D) at 640 nm (black) and 610 (red) nm in the presence of increasing concentration of SDS. Protein concentration is 7.2 μM in 50 mM phosphate buffer plus 0.1 M NaCl solution (pH = 7.3), T = 25 °C. The error associated with the reported data is of the same order of magnitude or smaller than the size of the points in the graph. (For interpretation of the references to colour in this figure legend, the reader is referred to the web version of this article.)

HS2 (featuring the Soret and CT bands at 403 and 610 nm), which is the only protein form observed at [SDS] = 10 mM.

The spectral changes observed for the wt protein are similar to those observed for the C46AC55A mutant (Fig. 2 A and B and Figs. 4 A, B), indicating that the same SDS-induced conformational changes occur, although at higher SDS concentration. Indeed, conversion of the low spin form into HS1 and of HS1 into HS2 occurs over a broader range of SDS concentrations, corresponding to those characterized by different slopes in Fig. S2 A. Moreover, the latter conformational transition begins at higher SDS concentrations than in the C46AC55A mutant (2.5 mM vs. 1.7 mM) and occurs before the full conversion of the low spin form into HS1. Therefore, for [SDS] ≥ 2.5 mM at least three protein conformations coexist in solution, as weak spectral signatures of the low spin and the HS1 forms are still observed in the presence of 10 mM SDS.

Hence, disruption of the Cys46-Cys55 disulfide bond facilitates the formation of the HS1 and HS2 forms, whereas it does not sensibly affect SDS-induced modifications of the out-of-plane deformations of the LS heme. This is a rather unexpected result, since cleavage of the disulfide bridge is reported to strengthen the bond between Fe(III) and the distal histidine [5,16,19,22,23]. As SDS-induced deformations of the LS heme occur for [SDS] ≤ 1 mM, well below the CMC, they appear to be triggered by SDS monomers, which effectively interact with hNgb altering its heme environment. Moreover, the affinity of SDS monomers for hNgb is almost independent of the Cys46-Cys55 disulfide bond, suggesting that the CD loop in not involved in SDS binding. Unfortunately, the present data do not clarify the molecular origin of the SDS-induced changes of the out-of-plane deformations of the LS heme, although in principle they could result either from a repositioning of the heme within the heme cavity due to the SDS-induced relaxing of the structural constraints blocking heme sliding [80,81], or from the replacement of the distal His64 by the amino group of the sidechain of Lys67, as observed for the H64V and H64L hNgb mutants at slightly alkaline pH values [82,83].

The 2nd derivative spectra confirm beyond doubt that formation of the HS1 and HS2 conformers occurs in the presence of SDS concentrations below and above the CMC (2-3 mM), respectively (Figs. 3 C, D and Fig. 4). The spectroscopic signatures of the HS1 and HS2 conformers of hNgb wt and its C46AC55A mutant closely remind those of the two high spin species formed by ferric horse metmyoglobin in the presence of 7 mM and 0.1 M SDS, respectively [42], suggesting similar heme axial coordination. The spectrum of HS1 rules out the presence of a six-coordinate HS heme with a His/H_2O axial coordination and is quite different from those of five-coordinate HS heme proteins featuring a His/- axial coordination, thereby making any suggestion about the identity of the Fe(III) axial ligands highly hypothetical. On the other hand, the spectroscopic properties of HS2 are closely similar to those of ferric metmyoglobin [42] and Fe-protoporphyrin IX [84] in the presence of high SDS concentrations and of the ferric H93G mutant of sperm whale myoglobin at pH 10.5 [85,86], indicating the presence of a 5-coordinate HS heme featuring a hydroxyl ion as the fifth ligand. Interestingly, the width and the shape of the trough associated to CT1 in the 2nd derivative spectra of HS2 raise the possibility that it could be actually composed by two closely spaced absorption bands, possibly arising from transitions into the d_{xz} and the d_{yz} orbitals of Fe(III). Therefore, it turns out that the distal His64 dissociates from Fe(III) at SDS concentration below the CMC, whereas interaction of hNgb with SDS micelles induces the rupture of the proximal axial bond between Fe(III) and His96, resulting in a complete detachment of the heme from the protein, as observed for ferric metmyoglobin for [SDS] > 9 mM [42]. As fluorescence spectra show that no apo-protein is formed up to 10 mM SDS (see

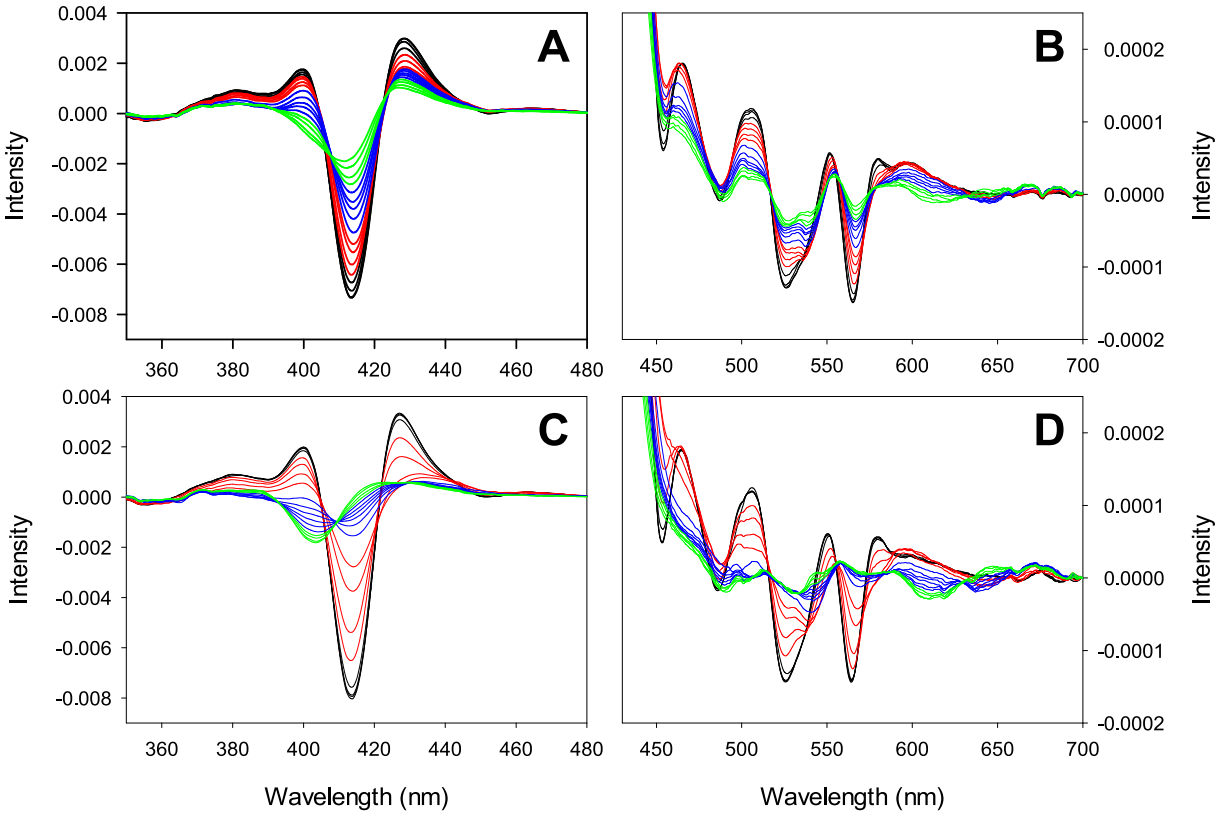

Fig. 4. 2nd derivative electronic absorption spectra of hNgb wt (A, B) and its C46AC55A mutant (C, D) in the presence of increasing SDS concentrations: 0 ≤ [SDS] ≤ 0.3 mM, black; 0.4 ≤ [SDS] ≤ 1.0 mM, red; 1.5 ≤ [SDS] ≤ 4.0 mM, blue; 5.0 ≤ [SDS] ≤ 10.0 mM, green. Protein concentration is 7.2 μM in 50 mM phosphate buffer plus 0.1 M NaCl solution (pH = 7.3), T = 25 °C. (For interpretation of the references to colour in this figure legend, the reader is referred to the web version of this article.)

below), it turns out that the detached heme is not released in solution. Most importantly, our data demonstrate that cleavage of the Cys46-Cys55 disulfide bond significantly facilitates heme detachment compared to hNgb wt.

Comparison of the 3D structures of the two proteins shows that their overall surface charge distribution is not significantly altered by the deletion of the disulfide bridge (Fig. S3), suggesting that the higher sensitivity to SDS of the C46AC55A species does not result from an increased electrostatic interaction between the negatively charged sulfate groups of SDS and the mutant. Indeed, it could be possibly related to a decreased stability of its 3D structure compared to the wt protein, in agreement with the observation that engineering of a second non-native disulfide bond in the A15C mutant of hNgb sensibly enhances the resistance to both Gdn-HCl-induced and pH-induced unfolding as well as the half denaturation temperature (Tm) compared to the wt protein, containing the single Cys46-Cys55 disulfide bond [87].

3.2. *Far-UV CD spectra*

The far-UV CD spectra of hNgb wt and of the C46AC55A mutant at

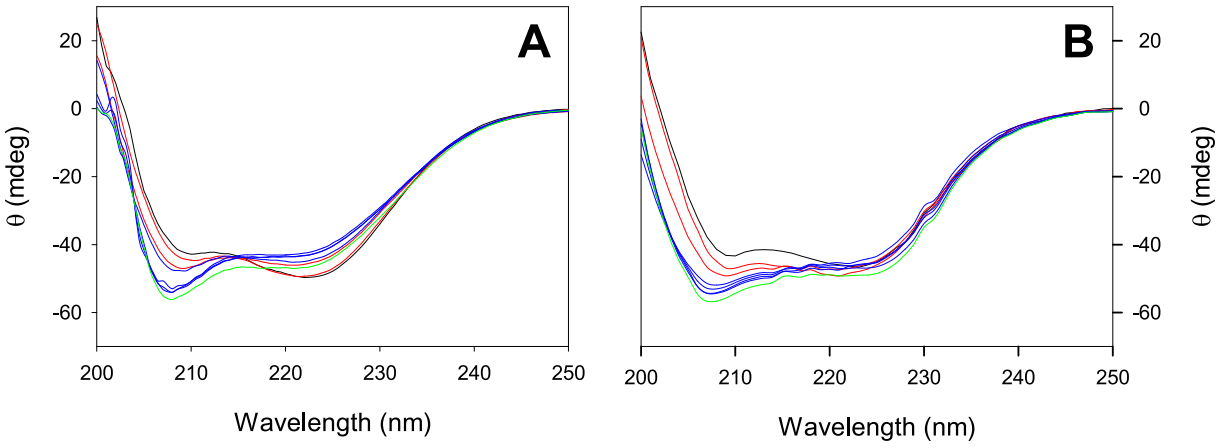

Fig. 5. Far Uv-CD spectra of wt hNgb wt (A) and its C46AC55A mutant (B) in the presence of increasing SDS concentrations: [SDS] = 0 mM, black; 0.4 ≤ [SDS] ≤ 1.0 mM, red; 1.5 ≤ [SDS] ≤ 4.0 mM, blue; [SDS] = 6.0 10.0 mM, green. Protein concentration is 1.125 μM in 5 mM HEPES buffer plus 0.1 M NaCl, (pH = 7.3), T = 25 °C. (For interpretation of the references to colour in this figure legend, the reader is referred to the web version of this article.)

pH 7.0 are similar, featuring the two negative bands typical of α-helical structures, at 212 (shoulder)/222 nm and at 209/223 nm for the wt protein and the C46AC55A mutant, respectively (Fig. 5). In the presence of increasing SDS concentration, the CD spectrum of both proteins progressively changes, as the intense negative band at 222-223 nm decreases considerably becoming a shoulder, while that at 209-212 nm gets deeper and red shifts to 208 nm (Fig. 5).

The BeStSel software (Beta Structure Selection, ELTE Eötvös Loránd University, Budapest, Hungary) [58] was used to analyze the CD spectra recorded at different SDS concentration and to determine effect of the denaturant on the secondary structure of hNgb wt and C46AC55A. The resulting distributions of the secondary structures as a function of SDS concentration are reported in Fig. 6 and show that, although in both cases a significant decrease in α-helix structures coupled with an increase of random structures occurs at increasing SDS concentration, remarkable differences exist between the wt protein and the C46AC55A mutant.

Indeed, hNgb wt experiences a progressive decrease of the α-helix fraction, which converts into a loop/random structure up to [SDS] = 1 mM and into β-sheet structures for 1 mM ≤ [SDS] ≤ 3 mM. Although only small changes in secondary structures are observed for SDS concentration between 3 and 4 mM SDS, the fraction of loop/random structures further increases at the detriment of both α-helix and β-sheet at SDS concentrations higher than 4 mM. The C46AC55A mutant shows a progressive and relevant decrease in α-helix structures at increasing SDS concentration which convert into loop/random structures with a minor β-sheet component, whose fraction remains almost unchanged at SDS concentration higher than 2 mM. The SDS-induced conversion of α-helices into loop/random structures occurs in three consecutive steps characterized by different slopes (Fig. 6B) occurring for [SDS] ≤ 1 mM, for 1 mM ≤ [SDS] ≤ 2 mM and for [SDS] ≥ 2 mM. Most importantly, these intervals coincide with those in which the SDS-induced deformations of the low heme of LS1, the LS1-to-HS1 and the HS1-to-HS2 transitions occur, clearly indicating that SDS-induced changes in the electronic properties of the heme in the C46AC55A mutant are coupled with significant changes in protein secondary structure. In particular, alterations of the out-of-plane deformations of the low heme of LS1 are associated with a limited α-helical unfolding, whereas conversion of the latter into the high spin HS1 species is accompanied by the conversion of a significant fraction of α-helices into loop/random structures and the formation of some β-sheets. Finally, the HS1-to-HS2 transition induces a relevant unfolding of the α-helices into loop/random structures.

The above interpretation extends to the SDS-induced changes in the secondary structure elements of the wt protein (Fig. 6A). Indeed, the relevant α-helical unfolding and the increase of the fraction of loop/random structures detected respectively for 1 mM ≤ [SDS] ≤ 3 mM and [SDS] ≥ 4 mM occur in the same range of SDS concentration of the SDS-induced LS1-to-HS1 and LS1/HS1-to-HS2 transitions, respectively. Compared to the C46AC55A mutant, the LS1-to-HS1 transition is associated with a far greater increase of the fraction of β-sheets, indicating that the deletion of the disulfide bond significantly influences the corresponding SDS-induced changes of the neuroglobin secondary structure. This difference almost disappears in the presence of higher SDS concentration, as in both cases the formation of the HS2 is associated with the unfolding of α-helices and β-sheets. In particular, the higher fraction of α-helices detected for the wt protein in the presence of 6 mM SDS fits with the presence of a non-negligible amount of low spin and HS1 species, indicated by the UV–vis spectra.

3.3. Fluorescence spectra

The fluorescence spectrum of wild type hNgb, obtained by selective excitation of tryptophans at 295 nm (Fig. S4, black spectrum), presents a maximum at 334 nm, in agreement with the different polarity/hydrophobicity of the protein environment surrounding the three tryptophan residues of hNgb: Trp133 is in a hydrophobic cavity, whereas Trp13 and Trp148 experience a more polar environment (Fig. 1). The spectrum of the C46AC55A mutant resembles that of the native form.

The fluorescence spectrum of hNgb wt, obtained when both Trps and Tyrs are excited at 280 nm, is only slightly blue-shifted compared to that obtained upon excitation at 295 nm (Fig. S4, red spectrum), with a maximum at about 332 nm. Moreover, it shows a very slight broadening in the wavelength range typical of tyrosine emission, whose maximum is at 303 nm [53]. Therefore, the quenching of Tyr fluorescence usually observed in proteins, due to electronic energy transfer to Trps [53], is very efficient also in hNgb, where the fluorescence of the four tyrosine residues results almost completely quenched. The fluorescence spectra of hNgb previously reported [88,89] are not directly comparable with ours, since the instrumental correction was not applied to the previously published spectra and a lower instrumental resolution was adopted.

The fluorescence emission in heme proteins, such as hemoglobin and myoglobin, has been considered undetectable by the standard spectrofluorometric instrumentations for many years, owing to the very efficient excitation energy transfer process from Trp to heme [53]. In hemoglobin, on the basis of the classical Förster theory for fluorescence resonance energy transfer (FRET) from Trp to heme, a fluorescence quenching ranging between 50 and 200 times compared to Trp in the absence of the heme acceptor, is expected [90]. However, by using front-

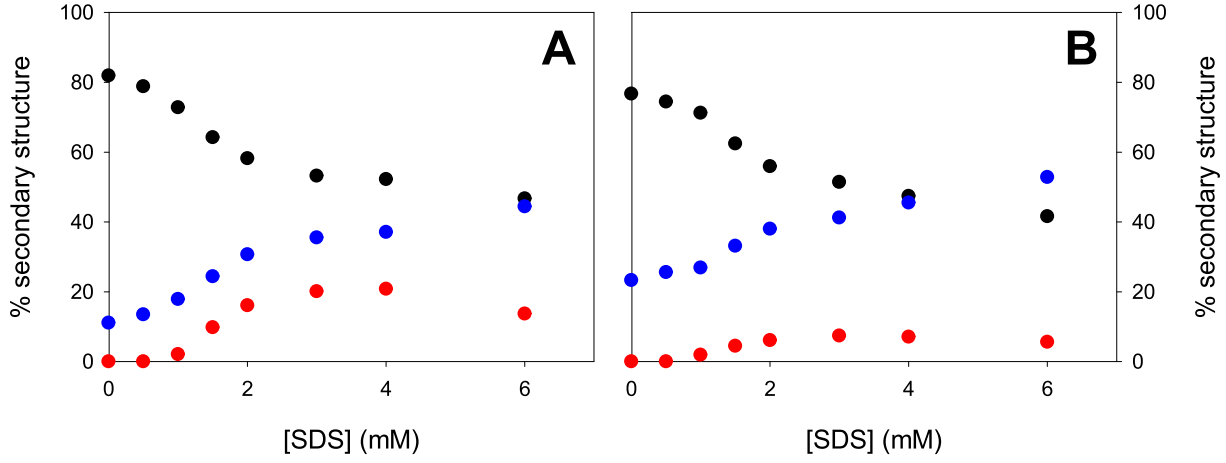

Fig. 6. Distribution curves of the secondary structures of hNgb wt (A) and its C46AC55A mutant (B) in the presence of increasing SDS concentration: α-helices, black; β-sheets, red; other (loops and random coils), blue. Protein concentration is 1.125 μM in 5 mM HEPES buffer plus 0.1 M NaCl, (pH = 7.3), T = 25 °C. (For interpretation of the references to colour in this figure legend, the reader is referred to the web version of this article.)

face fluorometry or alternative excitation sources, some authors were able to detect fluorescence emission from heme protein [91]. The calculated lifetimes are in the range of picoseconds, according to experimental values [90].

Analysis of the three-dimensional structures of wild type and C46AC55A hNgb (Fig. 1) reveals that in both cases Trp148 is the closest to the heme (7.8 Å), whereas the distances from the heme of Trp13 and Trp133 are 9.3 and 10.0 Å, respectively. These Trp-heme distances are shorter than the Förster distance for energy transfer (29 Å, see Introduction), which represents the distance at which FRET is 50 % efficient, i.e., the distance at which the energy transfer rate equals the decay rate of the donor. For shorter distances an increase in the energy transfer rate, depending on the reciprocal of the sixth power of the distance, is expected. The detectable fluorescence signal of hNgb wt and the C46AC55A mutant, observed using dilute samples and right-angle detection with standard fluorometric instrumentation (see Materials and Methods), differentiates hNgb from the other heme proteins, such as hemoglobin and myoglobin, suggesting a lower efficiency of electronic energy transfer from tryptophans to heme. The experimental fluorescence quantum yield, determined for both proteins, is 0.015. This value, corresponding to the average quantum yield of the individual tryptophan residues present in the protein, is quite low compared with those of other multi-tryptophan proteins [92]. Nevertheless, it indicates a lower efficiency of FRET compared to other heme proteins. The longer fluorescence lifetimes compared to hemoglobin and myoglobin (see below) support such hypothesis. The above cited value of Förster distance (R_0 = 29 Å) was calculated under the assumption of an orientation factor equal to 2/3 [56], i.e., the value calculated for couples of donors and acceptors that are randomly oriented, due to rotational diffusion (for an exhaustive discussion for the FRET theory, see ref. [53]). However, this assumption, i.e., a random orientation of the chromophores, does not hold in a folded protein where heme and tryptophans form a rigid donor-acceptor system [93]. Therefore, the more intense fluorescence emission in hNgb, compared to other heme proteins, can be explained hypothesizing that at least one among the three Trp residues in hNgb presents an orientation that reduces the rate of energy transfer to heme [91,94].

The changes in fluorescence spectra of hNgb wt induced by increasing concentration of SDS (0 mM - 1 mM) are shown in Fig. 7A, whereas the spectra obtained at higher SDS concentrations are shown in Fig. S5. The spectrum at [SDS] = 0.1 mM is superimposable with that obtained in the absence of SDS, with a maximum at 334 nm. For SDS concentrations 0.2-0.4 mM the spectrum is slightly blue-shifted, with a maximum at 331 nm; no further changes are observed for [SDS] $\geq$ 0.5 mM. The maximum of the fluorescence spectra of the C46AC55A mutant (Fig. 7B) blue-shifts from 335 nm in the absence of SDS to 331 nm at [SDS] = 0.4 mM and remains unchanged for higher SDS concentrations (Figs. 7B and S6). Therefore, for both species a hypsochromic shift is observed at SDS concentrations lower than CMC (about 2 mM [51]).

The SDS-induced changes of fluorescence intensity, monitored at 335 nm, in hNgb wt and the C46AC55A mutant are very different (Fig. S7). In the former case the fluorescence intensity increases between 0.1 and 0.3 mM and then remains essentially unchanged, whereas for the latter species a marked initial decrease up to [SDS] = 0.3 mM is observed, followed by an increase at higher SDS concentrations.

The changes in fluorescence spectra of HNgb suggest significant modifications of the secondary structure of both forms at increasing concentrations of SDS in the submicellar concentration of SDS. The maximum of the fluorescence spectra shifts to the blue, unlike myoglobin [42] and cytochrome *c* [50], indicating that upon increasing SDS concentration Trps probe a more hydrophobic environment. The limited blue shift observed at low SDS concentrations (0.1-0.4 mM) could in principle arise from the specific interaction between Trp residues and hydrophobic tails of SDS, whereas at higher SDS concentrations, the hydrophobic nature of the environment that surrounds the protein could be due to the formation of SDS clusters/micelles.

The different SDS-induced changes in fluorescence intensity observed for hNgb wt and the C46AC55A mutant are consistent with the differences highlighted by the electronic and CD spectra. In particular, the SDS-induced changes of the fluorescence intensity of the C46AC55A mutant occur in the same ranges of SDS concentrations of the conformational transitions altering the electronic properties of the heme iron and the protein secondary structure, suggesting that they arise from the same molecular factors. Indeed, the increase in fluorescence emission observed for [SDS] > 0.4 mM are consistent with the progressive SDS-induced protein unfolding. The decrease in emission observed for [SDS] $\leq$ 0.4 mM indicates that the initial SDS-induced deformation of the low spin heme of LS1 enhances the efficiency of electronic energy transfer from tryptophans to heme in the C46AC55A mutant.

3.4. *Fluorescence lifetimes and fluorescence anisotropy*

The fluorescence decay parameters for hNgb wt and the C46AC55A mutant were determined at emission wavelengths of 320 and 340 nm. The results are reported in Tables S2 and S3. The best fit was obtained in all cases with a triple-exponential decay function. The native protein and the mutant feature similar decay, as in both cases three components can be identified. In particular, two longer-lived components, with lifetimes near 2-2.5 and 6-7 ns, respectively, and one faster decay, with a lifetime close to 0.5 ns were observed. The average lifetime is 1.1 ns and 1.6 ns at emission wavelength of 320 nm and 340 nm, respectively.

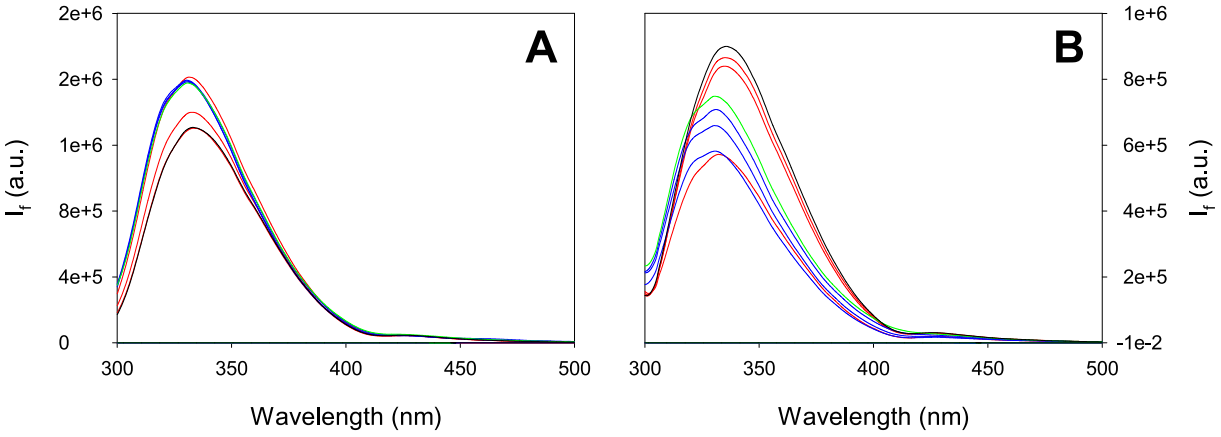

Fig. 7. Fluorescence spectra of hNgb wt (A) and its C46AC55A mutant (B) in the presence of increasing SDS concentrations (0-1 mM): [SDS] = 0 mM, black; 0.1 $\leq$ [SDS] $\leq$ 0.3 mM, red; 0.4 $\leq$ [SDS] $\leq$ 0.75 mM, blue; [SDS] = 1.0 mM, green. 50 mM phosphate buffer plus 0.1 M NaCl solution (pH = 7.3), T = 25 °C. (For interpretation of the references to colour in this figure legend, the reader is referred to the web version of this article.)

The time-resolved measurements of multi-tryptophan proteins lead to very complex decays. This observation can be partly understood considering that Trp itself and proteins containing a single tryptophan residue display a multiexponential fluorescence decay, arising from the existence of different microstates for each Trp in the ground state, due to the presence of different rotamers or different conformations of adjacent side chains of other residues. [95]. Therefore, the fluorescence properties of each Trp in proteins are influenced by different local environments.

Heme proteins are generally characterized by very short fluorescence lifetimes, due to very efficient energy transfer processes from Trp residues to heme. In cytochrome *c* and in hemoglobin the dominant component is characterized by a decay time near 20 ps [50,96]. Although the instrumental resolution (100 ps) does not allow us to measure a possible decay of this extent, fluorescence lifetimes values of hNgb are consistent with the measured value of fluorescence quantum yield, confirming a reduced efficiency of energy transfer process in this protein.

Further insights into the conformational changes of hNgb and C46AC55A can be obtained by the analysis of the fluorescence emission anisotropy (Figs. S8 and S9). The interaction of the two proteins with SDS is confirmed to be a multistep process. The average anisotropy values r progressively decrease for SDS concentrations approximately higher than 0.4-0.5 mM (Tables S4 and S5). Considering that the decay lifetimes remain nearly constant, on the basis of the Perrin Equation [97], the depolarization of fluorescence emission of Trps at SDS concentration higher than 0.5 mM can be assigned to an increase of their rotational correlation times, θ, i.e., to a higher flexibility, in agreement with the hypothesis of the SDS-induced unfolding of hNgb. These observations are consistent with the marked change in the secondary structure, corresponding to the LS-HS transition, observed for SDS concentrations higher than 0.5 mM with electronic absorption and CD spectra, which leads to the unfolding of the protein.

3.5. Effects of hydrogen peroxide on the electronic absorption spectra of wt and mutated hNgb

hNgb wt and the C46AC55A mutant were found to undergo H_2O_2-induced degradation of the heme center at very slow rate [25,26]. This process can be conceivably related to the presence of a minor amount of five-coordinate heme, which is the only species able to react with H_2O_2 to yield the hydroperoxo derivative and eventually the ferryl center needed for heme degradation. The increase in the high-to-low spin molar ratio observed with increasing SDS concentration, therefore, should reasonably lead to an increase in the reactivity towards H_2O_2 of HNgb wt and its C46AC55A mutant.

Fig. S10 shows selected UV–Vis spectra of hNgb wt and its C46AC55A mutant recorded over time in the presence of different SDS concentrations after addition of 200 μM H_2O_2, which mimics an acute/transitory (on the timescale of minutes/h) condition of extracellular oxidative stress [64]. It turns out that in the presence of SDS, the absorbance of the Soret and Q bands decrease with time due to heme degradation and no new signal appears, although above 0.5 mM SDS the Soret band broadens and red shifts (Fig. S10). The time course of the Abs_{413} decrease follows a pseudo 1st order kinetics only in absence or at low concentration of SDS, according to $A = A_1\, e^{-k1t}$ (Eq. 2) (Fig. S11 A, B) [25,26]. When the SDS concentration increases above 0.2 mM the dependence of absorbance vs. time is more complex and shows a biphasic behavior (Fig. S11 C—F), suggesting that the degradation process involves two protein forms characterized by different degradation kinetics. This is consistent with the observed broadening and shifting of the Soret band.

To obtain the rate constants associated with each reaction, the biphasic time-dependent absorbance changes at 413 nm were fitted to:

$$A = A_1\, e^{-k1t} + A_2\, e^{-k2t} \quad (3)$$

where A_1 and A_2 are the initial absorbance associated with the two consecutive phases (starting species), and k_1 and k_2 are the corresponding rate constants of the oxidative degradation. The kinetic constants determined at different SDS concentrations show that the rate of heme degradation appreciably increases with increasing SDS concentration (Table 1, Fig. 8).

3.6. Kinetics and mechanism of H_2O_2-induced heme degradation in hNgb

The physiological role(s) of hNgb is(are) not yet fully understood [2,3,98–102], although the protection of neurons and retinal cells from oxidative stress by ROS is one of the most probable functions [2,3,103]. Although the details of this activity still remain unknown, it could involve processes that can lead to heme degradation, as observed for other globins [104–107]. The oxidative degradation mechanism due to H_2O_2 proposed for myoglobin and hemoglobin involves the oxidation of ferrous or ferric heme by hydrogen peroxide (or peroxides) to form a ferryl species. The latter, in the absence of substrate, leads to the oxidation of the heme itself due to its high reactivity [108,109]. For hNgb, a similar mechanism reasonably occurs [25,26], although it's not clear to what extent it is related to the protein's physiological role. Notably, it is worth noting that an dysregulated peroxidase activity can cause severe cellular damage [62–66]. The presence of the two axial His heme iron ligands and the steric hindrance of the polypeptide matrix, however, avoid the formation of the ferryl group which however can be easily formed by the high-spin penta-coordinated minor form [25,26,110,111]. This fact and the slow kinetics for the low-spin→high-spin conversion could be the causes of the high resistance of hNgb to H_2O_2-induced oxidative stress and of the extremely slow rate of heme degradation observed in solution [25,26]. The accessibility of the heme center to the solvent has also been proposed as a factor regulating the protein/H_2O_2 interaction kinetics. Indeed, it was observed that heme accessibility and oxidative degradation kinetics of hNgb significantly decrease upon removal of the disulfide bridge that closes the heme cleft [1–4,6,14–17,19–28]. The presence or absence of the disulfide bridge as well as the functionality of the protein have been related to oxidizing or reducing conditions of physiological or pathological states of the cell [10,18,20,112]. Understanding the role played by the intramolecular disulfide bond in H_2O_2 reactivity is therefore essential to gain information on the oxidative stress-related processes possibly involving the protein in the organism, since the chemical inertia of both hNgb forms towards H_2O_2 apparently conflicts with the proposed role of ROS scavenger, pointing to a more complex involvement in cellular response to oxidative stress [2,3,8–10].

In the presence of SDS, however, the response towards H_2O_2 of the wt protein and the C46AC55A mutant changes considerably. Indeed, both proteins show a progressive and significant increase in the rate of oxidative degradation. The time course of the decreases in absorbance of the Soret band obtained at [SDS] > 0.2 mM is clearly biphasic,

Table 1
Pseudo-1st order kinetic constants for H_2O_2-induced heme degradation for hNgb wt and its C46AC55A mutant in the presence of SDS (0-3 mM) and 200 μM H_2O_2.[a]

	wt hNgb		C46AC55A hNgb	
[SDS]/mM	k_1/min^{-1}	k_2/min^{-1}	k_1/min^{-1}	k_2/min^{-1}
0	0.0029	–	0.0019	–
0.2	0.0056	–	0.0089	–
0.5	0.013	0.082	0.016	0.17
1	0.018	0.27	0.025	0.45
2	0.021	0.38	0.037	0.68
3	0.022	0.38	0.042	0.79

[a] Values obtained from the plots shown in Fig. S11. The k_I and k_{II} values are affected by an error of about ±8 %. Protein concentration: 3-5 μM, 50 mM phosphate buffer plus 0.1 M NaCl, pH 7.4. $T = 25$ °C.

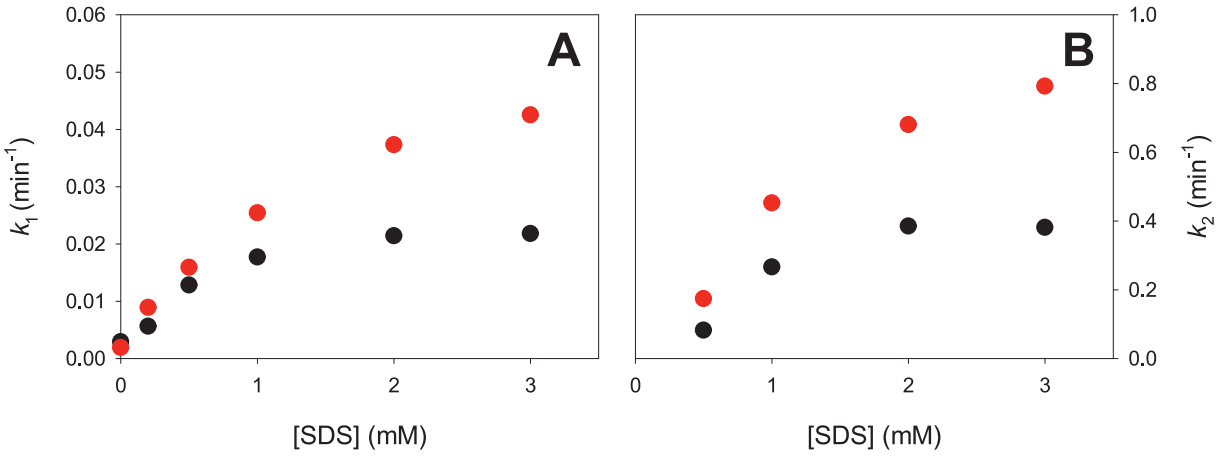

Fig. 8. Changes in the kinetic constants for H_2O_2-induced heme degradation k_1 (A) and k_2 (B) in the presence of increasing concentration of SDS at pH 7.4 and T = 25 °C for hNgb wt (black) and its C46AC55A mutant (red). The error associated with the reported data is of the same order of magnitude or smaller than the size of the points in the graph. (For interpretation of the references to colour in this figure legend, the reader is referred to the web version of this article.)

suggesting that at least two different protein forms are involved in the oxidative degradation process featuring significantly different kinetics. Comparison of the kinetic results with the conformational information obtained from electronic, far UV CD and fluorescence spectra support the hypothesis that the two trends observed for the oxidative degradation kinetics arise from two high spin (five-coordinated) species resulting from a different number of protein-bound SDS molecules. The most significant increase in the rate of H_2O_2-induced heme degradation in hNgb is observed at SDS concentrations below CMC, thus confirming the fundamental role played by SDS monomers not only on protein conformation and heme structure, but also on the reactivity towards H_2O_2.

The different effect of increasing SDS concentration on the kinetics of the oxidative degradation process in wt hNgb and its C46AC55A mutant is fully consistent with the different SDS-induced changes in protein conformation and heme electronic properties. Indeed, the comparable k_1 and k_2 values featured by both proteins up to [SDS] = 1 mM are consistent with the fact that both species undergo to the same SDS-induced modifications of the heme out-of-plane deformations of LS1 and to the progressive conversion of α-helices into loop/random structures. On the other hand, the higher k_1 and k_2 values of the C46AC55A mutant for [SDS] $\geq$ 1 mM fit with its increased sensitivity to the denaturant effect of SDS compared to the wt protein, which result in the formation of a much higher amount of the HS1 and HS2 conformers and in a massive conversion of α-helices into loop/random structures. Indeed, the formation of the HS2 conformer of the wt species begins at [SDS] $\geq$ 2.5 mM, in agreement with the invariance of its k_1 and k_2 values for 2 and 3 mM SDS.

4. Conclusions

SDS causes appreciable conformational changes in hNgb wt and its C46AC55A mutant already at low concentrations. The relevant SDS-induced modifications of the secondary structure affect both the heme group and Trp residues, as indicated by absorption and fluorescence spectra, respectively. Absorption spectra indicates that the addition of SDS induces the detachment of the distal histidine and the resulting formation of two high-spin (pentacoordinate) species (HS1 and HS2) observed at different SDS concentrations, the latter of which contains an unbound heme. The unfolding induced by SDS occurs through different processes for the two proteins. The C46AC55A mutant shows a strong propensity to form loop/random structures already at low SDS concentrations (>0.5 mM), whereas in the same conditions the wt protein contains a high amount of β-sheet. The higher sensitivity to SDS of the former does not result from an increased electrostatic interaction with the negatively charged sulfate groups of SDS, as the deletion of the disulfide bridge does not significantly modify the overall surface charge distribution (Fig. S3), and it is possibly related to a decreased stability of 3D structure of the C46AC55A mutant.

The different evolution of fluorescence spectra of hNgb wt and the C46AC55A mutant at SDS concentrations lower than 0.5 mM suggests different changes in the initial step of interaction with SDS which affect environment of the triptophan residue(s), but do not modify appreciably protein folding and the heme coordination sphere of the two hNgb. The large changes observed in the secondary structure of the proteins and the increase in high-spin forms due to SDS binding make the heme center more susceptible to H_2O_2-induced degradation. Deletion of the Cys46-Cys55 disulfide bridge heavily enhances the sensitivity of hNgb to SDS, since it favors the formation of the high spin conformers HS1 and HS2 (which are observed at lower SDS concentrations) as well as the conversion of α-helices to loop/random structures, resulting in an increased reactivity towards H_2O_2.

CRediT authorship contribution statement

Monica Caselli: Writing – review & editing, Writing – original draft, Investigation, Funding acquisition, Formal analysis. **Lorenzo Sebastianelli:** Writing – original draft, Investigation, Formal analysis. **Mirco Meglioli:** Investigation, Formal analysis. **Gianantonio Battistuzzi:** Writing – review & editing, Writing – original draft, Funding acquisition, Conceptualization. **Marco Borsari:** Writing – review & editing, Writing – original draft, Supervision, Formal analysis, Conceptualization.

Funding information

This work was supported by the University of Modena and Reggio Emilia DSCG FAR2022 (MC) and DSCG FAR2021 (GB) funding programs.

Declaration of competing interest

The authors declare that they have no known competing financial interests or personal relationships that could have appeared to influence the work reported in this paper.

Appendix A. Supplementary data

Supplementary data to this article can be found online at https://doi.org/10.1016/j.jinorgbio.2025.113109.

Data availability

Data will be made available on request.

References

[1] M. Bellei, C.A. Bortolotti, G. Di Rocco, M. Borsari, L. Lancellotti, A. Ranieri, M. Sola, G. Battistuzzi, The influence of the Cys46/Cys55 disulfide bond on the redox and spectroscopic properties of human neuroglobin, J. Inorg. Biochem. 178 (2018) 70–86, https://doi.org/10.1016/j.jinorgbio.2017.10.005.

[2] P. Ascenzi, A. di Masi, L. Leboffe, M. Fiocchetti, M.T. Nuzzo, M. Brunori, M. Marino, Neuroglobin: from structure to function in health and disease, Mol. Asp. Med. 52 (2016) 1–48, https://doi.org/10.1016/j.mam.2016.10.004.

[3] G. De Simone, D. Sbardella, F. Oddone, A. Pesce, M. Coletta, P. Ascenzi, Structural and (Pseudo-)enzymatic properties of Neuroglobin: its possible role in neuroprotection, Cells 10 (2021) 3366, https://doi.org/10.3390/cells10123366.

[4] P. Picotti, S. Dewilde, A. Fago, C. Hundahl, V. De Filippis, L. Moens, A. Fontana, Unusual stability of human neuroglobin at low pH - molecular mechanisms and biological significance, FEBS J. 276 (2009) 7027–7039, https://doi.org/10.1111/j.1742-4658.2009.07416.x.

[5] D. Hamdane, L. Kiger, S. Dewilde, B.N. Green, A. Pesce, J. Uzan, T. Burmester, T. Hankeln, M. Bolognesi, L. Moens, M.C. Marden, Coupling of the Heme and an Internal Disulfide Bond in Human Neuroglobin, in: Micron, Elsevier Ltd, 2004, pp. 59–62, https://doi.org/10.1016/j.micron.2003.10.019.

[6] A. Pesce, S. Dewilde, M. Nardini, L. Moens, P. Ascenzi, T. Hankeln, T. Burmester, M. Bolognesi, Human brain neuroglobin structure reveals a distinct mode of controlling oxygen affinity, Structure 11 (2003) 1087–1095, https://doi.org/10.1016/S0969-2126(03)00166-7.

[7] C. Zhang, C. Gao, J. Mu, Z. Qiu, L. Li, Spectroscopic studies on unfolding processes of apo-neuroglobin induced by guanidine hydrochloride and urea, Biomed. Res. Int. 2013 (2013), https://doi.org/10.1155/2013/349542.

[8] M. Fiocchetti, V.S. Fernandez, E. Montalesi, M. Marino, Neuroglobin: a novel player in the oxidative stress response of cancer cells, Oxidative Med. Cell. Longev. 2019 (2019), https://doi.org/10.1155/2019/6315034.

[9] C. Exertier, L.C. Montemiglio, I. Freda, E. Gugole, G. Parisi, C. Savino, B. Vallone, Neuroglobin, clues to function and mechanism, Mol. Asp. Med. 84 (2022), https://doi.org/10.1016/j.mam.2021.101055.

[10] M.A. Semenova, R.V. Chertkova, M.P. Kirpichnikov, D.A. Dolgikh, Molecular interactions between Neuroglobin and cytochrome c: possible mechanisms of Antiapoptotic defense in neuronal cells, Biomolecules 13 (2023), https://doi.org/10.3390/biom13081233.

[11] A. Fago, C. Hundahl, S. Dewilde, K. Gilany, L. Moens, R.E. Weber, Allosteric regulation and temperature dependence of oxygen binding in human neuroglobin and cytoglobin: molecular mechanisms and physiological significance, J. Biol. Chem. 279 (2004) 44417–44426, https://doi.org/10.1074/jbc.M407126200.

[12] J. Tejero, C.E. Sparacino-Watkins, V. Ragireddy, S. Frizzell, M.T. Gladwin, Exploring the mechanisms of the reductase activity of neuroglobin by site-directed mutagenesis of the heme distal pocket, Biochemistry 54 (2015) 722–733, https://doi.org/10.1021/bi501196k.

[13] A. Fago, C. Hundahl, H. Malte, R.E. Weber, Functional properties of neuroglobin and cytoglobin. Insights into the ancestral physiological roles of globins, in: IUBMB Life, 2004, pp. 689–696, https://doi.org/10.1080/15216540500037299.

[14] B.G. Guimarães, D. Hamdane, C. Lechauve, M.C. Marden, B. Golinelli-Pimpaneau, The crystal structure of wild-type human brain neuroglobin reveals flexibility of the disulfide bond that regulates oxygen affinity, Acta Crystallogr. D Biol. Crystallogr. 70 (2014) 1005–1014, https://doi.org/10.1107/S1399004714000078.

[15] A.D. Nadra, M.A. Martí, A. Pesce, M. Bolognesi, D.A. Estrin, Exploring the molecular basis of heme coordination in human neuroglobin, proteins: structure, Function and Genetics 71 (2008) 695–705, https://doi.org/10.1002/prot.21814.

[16] A.N. Morozov, J.P. Roach, M. Kotzer, D.C. Chatfield, A possible mechanism for redox control of human neuroglobin activity, J. Chem. Inf. Model. 54 (2014) 1997–2003, https://doi.org/10.1021/ci5002108.

[17] M. Ezhevskaya, F. Trandafir, L. Moens, S. Dewilde, S. Van Doorslaer, EPR investigation of the role of B10 phenylalanine in neuroglobin - evidence that B10Phe mediates structural changes in the heme region upon disulfide-bridge formation, J. Inorg. Biochem. 105 (2011) 1131–1137, https://doi.org/10.1016/j.jinorgbio.2011.05.020.

[18] D. Hamdane, L. Kiger, S. Dewilde, B.N. Green, A. Pesce, J. Uzan, T. Burmester, T. Hankeln, M. Bolognesi, L. Moens, M.C. Marden, The redox state of the cell regulates the ligand binding affinity of human Neuroglobin and Cytoglobin, J. Biol. Chem. 278 (2003) 51713–51721, https://doi.org/10.1074/jbc.M309396200.

[19] S. Trashin, M. De Jong, E. Luyckx, S. Dewilde, K. De Wael, Electrochemical evidence for neuroglobin activity on NO at physiological concentrations, J. Biol. Chem. 291 (2016) 18959–18966, https://doi.org/10.1074/jbc.M116.730176.

[20] M. Tiso, J. Tejero, S. Basu, I. Azarov, X. Wang, V. Simplaceanu, S. Frizzell, T. Jayaraman, L. Geary, C. Shapiro, C. Ho, S. Shiva, D.B. Kim-Shapiro, M. T. Gladwin, Human neuroglobin functions as a redox-regulated nitrite reductase, J. Biol. Chem. 286 (2011) 18277–18289, https://doi.org/10.1074/jbc.M110.159541.

[21] S. Nicolis, E. Monzani, C. Ciaccio, P. Ascenzi, L. Moens, L. Casella, Reactivity and endogenous modification by nitrite and hydrogen peroxide: does human neuroglobin act only as a scavenger? Biochem. J. 407 (2007) 89–99, https://doi.org/10.1042/BJ20070372.

[22] A. Bocahut, V. Derrien, S. Bernad, P. Sebban, S. Sacquin-Mora, E. Guittet, E. Lescop, Heme orientation modulates histidine dissociation and ligand binding kinetics in the hexacoordinated human neuroglobin, J. Biol. Inorg. Chem. 18 (2013) 111–122, https://doi.org/10.1007/s00775-012-0956-2.

[23] L. Astudillo, S. Bernad, V. Derrien, P. Sebban, J. Miksovska, Probing the role of the internal disulfide bond in regulating conformational dynamics in Neuroglobin, Biophys. J. 99 (2010) L16–L18, https://doi.org/10.1016/j.bpj.2010.04.033.

[24] A. Bocahut, S. Bernad, P. Sebban, S. Sacquin-Mora, Relating the diffusion of small ligands in human neuroglobin to its structural and mechanical properties, J. Phys. Chem. B 113 (2009) 16257–16267, https://doi.org/10.1021/jp906854x.

[25] G. Di Rocco, F. Bernini, G. Battistuzzi, A. Ranieri, C.A. Bortolotti, M. Borsari, M. Sola, Hydrogen peroxide induces heme degradation and protein aggregation in human neuroglobin: roles of the disulfide bridge and hydrogen-bonding in the distal heme cavity, FEBS J. 290 (2023) 148–161, https://doi.org/10.1111/febs.16581.

[26] A. Cassiani, P.G. Furtmüller, M. Borsari, G. Battistuzzi, S. Hofbauer, Insights into heme degradation and hydrogen peroxide-induced dimerization of human neuroglobin, Biosci. Rep. 45 (2025) 1–13, https://doi.org/10.1042/BSR20241265.

[27] E. Vinck, S. Van Doorslaer, S. Dewilde, L. Moens, Structural change of the Heme pocket due to disulfide bridge formation is significantly larger for Neuroglobin than for Cytoglobin, J. Am. Chem. Soc. 126 (2004) 4516–4517, https://doi.org/10.1021/ja0383322.

[28] H. Ishikawa, S. Kim, K. Kwak, K. Wakasugi, M.D. Fayer, Disulfide bond influence on protein structural dynamics probed with 2D-IR vibrational echo spectroscopy, Proc. Natl. Acad. Sci. 104 (2007) 19309–19314, https://doi.org/10.1073/pnas.0709760104.

[29] M.N. Jones, Surfactant interactions with biomembranes and proteins, Chem. Soc. Rev. 21 (1992) 127, https://doi.org/10.1039/cs9922100127.

[30] D. Winogradoff, S. John, A. Aksimentiev, Protein unfolding by SDS: the microscopic mechanisms and the properties of the SDS-protein assembly, Nanoscale 12 (2020) 5422–5434, https://doi.org/10.1039/C9NR09135A.

[31] G. Krainer, A. Hartmann, V. Bogatyr, J. Nielsen, M. Schlierf, D.E. Otzen, SDS-induced multi-stage unfolding of a small globular protein through different denatured states revealed by single-molecule fluorescence, Chem. Sci. 11 (2020) 9141–9153, https://doi.org/10.1039/d0sc02100h.

[32] A. Das, C. Mukhopadhyay, Urea-mediated protein denaturation: a consensus view, J. Phys. Chem. B 113 (2009) 12816–12824, https://doi.org/10.1021/jp906350s.

[33] G.D. Rose, P.J. Fleming, J.R. Banavar, A. Maritan, A backbone-based theory of protein folding, Proc. Natl. Acad. Sci. USA 103 (2006) 16623–16633, https://doi.org/10.1073/pnas.0606843103.

[34] X. Hoccart, G. Turrell, Raman spectroscopic investigation of the dynamics of urea–water complexes, J. Chem. Phys. 99 (1993) 8498–8503, https://doi.org/10.1063/1.465626.

[35] R.D. Macdonald, M. Khajehpour, Effects of the protein denaturant guanidinium chloride on aqueous hydrophobic contact-pair interactions, Biophys. Chem. 196 (2015) 25–32, https://doi.org/10.1016/j.bpc.2014.08.006.

[36] A. Huerta-Viga, S. Woutersen, Protein denaturation with guanidinium: a 2D-IR study, J. Phys. Chem. Lett. 4 (2013) 3397–3401, https://doi.org/10.1021/jz401754b.

[37] D. Otzen, Protein–surfactant interactions: a tale of many states, Biochimica et Biophysica Acta (BBA) - Proteins and Proteomics 1814 (2011) 562–591, https://doi.org/10.1016/j.bbapap.2011.03.003.

[38] J.H. Hansen, S.V. Petersen, K.K. Andersen, J.J. Enghild, T. Damhus, D. Otzen, Stable intermediates determine proteins' primary unfolding sites in the presence of surfactants, Biopolymers 91 (2009) 221–231, https://doi.org/10.1002/bip.21125.

[39] M. Aguirre-Ramírez, H. Silva-Jiménez, I.M. Banat, M.A. Díaz De Rienzo, Surfactants: physicochemical interactions with biological macromolecules, Biotechnol. Lett. 43 (2021) 523–535, https://doi.org/10.1007/s10529-020-03054-1.

[40] S. Oellerich, H. Wackerbarth, P. Hildebrandt, Spectroscopic characterization of nonnative conformational states of cytochrome c, J. Phys. Chem. B 106 (2002) 6566–6580, https://doi.org/10.1021/jp013841g.

[41] N.J. Turro, X.-G. Lei, K.P. Ananthapadmanabhan, M. Aronson, Spectroscopic probe analysis of protein-surfactant interactions: the BSA/SDS system, Langmuir 11 (1995) 2525–2533, https://doi.org/10.1021/la00007a035.

[42] L. Tofani, A. Feis, R.E. Snoke, D. Berti, P. Baglioni, G. Smulevich, Spectroscopic and interfacial properties of myoglobin/surfactant complexes, Biophys. J. 87 (2004) 1186–1195, https://doi.org/10.1529/biophysj.104.041731.

[43] K.K. Andersen, P. Westh, D.E. Otzen, Global study of myoglobin - surfactant interactions, Langmuir 24 (2008) 399–407, https://doi.org/10.1021/la702890y.

[44] K.K. Andersen, C.L. Oliveira, K.L. Larsen, F.M. Poulsen, T.H. Callisen, P. Westh, J. S. Pedersen, D. Otzen, The role of decorated SDS micelles in sub-CMC protein denaturation and association, J. Mol. Biol. 391 (2009) 207–226, https://doi.org/10.1016/j.jmb.2009.06.019.

[45] M. Jafari, F. Mehrnejad, F. Rahimi, S.M. Asghari, The molecular basis of the sodium dodecyl sulfate effect on human ubiquitin structure: a molecular dynamics simulation study, Sci. Rep. 8 (2018), https://doi.org/10.1038/s41598-018-20669-7.

[46] A.K. Bhuyan, On the mechanism of SDS-induced protein denaturation, Biopolymers 93 (2010) 186–199, https://doi.org/10.1002/bip.21318.

[47] G.V. Jensen, R. Lund, J. Gummel, T. Narayanan, J.S. Pedersen, Monitoring the transition from spherical to polymer-like surfactant micelles using small-angle X-ray scattering, Angew. Chem. Int. Ed. 53 (2014) 11524–11528, https://doi.org/10.1002/anie.201406489.
[48] K. Schäfer, H.B. Kolli, M. Killingmoe Christensen, S.L. Bore, G. Diezemann, J. Gauss, G. Milano, R. Lund, M. Cascella, Supramolecular packing drives morphological transitions of charged surfactant micelles, Angew. Chem. Int. Ed. 59 (2020) 18591–18598, https://doi.org/10.1002/anie.202004522.
[49] A.G. Rocco, L. Mollica, P. Ricchiuto, A.M. Baptista, E. Gianazza, I. Eberini, Characterization of the protein unfolding processes induced by urea and temperature, Biophys. J. 94 (2008) 2241–2251, https://doi.org/10.1529/biophysj.107.115535.
[50] T.K. Das, S. Mazumdar, S. Mitra, Characterization of a partially unfolded structure of cytochrome *c* induced by sodium dodecyl sulphate and the kinetics of its refolding, Eur. J. Biochem. 254 (1998) 662–670, https://doi.org/10.1046/j.1432-1327.1998.2540662.x.
[51] E. Fuguet, C. Ràfols, M. Rosés, E. Bosch, Critical micelle concentration of surfactants in aqueous buffered and unbuffered systems, Anal. Chim. Acta 548 (2005) 95–100, https://doi.org/10.1016/j.aca.2005.05.069.
[52] M.R. Eftink, The use of fluorescence methods to monitor unfolding transitions in proteins, Biophys. J. 66 (1994) 482–501, https://doi.org/10.1016/S0006-3495(94)80799-4.
[53] J.R. Lakowicz, Principles of Fluorescence Spectroscopy, Springer US, Boston, MA, 2006, https://doi.org/10.1007/978-0-387-46312-4.
[54] N. Varejão, D. Reverter, Using Intrinsic Fluorescence to Measure Protein Stability upon Thermal and Chemical Denaturation, 2023, pp. 229–241, https://doi.org/10.1007/978-1-0716-2784-6_16.
[55] F.H. dos Santos Rodrigues, G.G. Delgado, T. Santana da Costa, L. Tasic, Applications of fluorescence spectroscopy in protein conformational changes and intermolecular contacts, BBA Advances 3 (2023) 100091, https://doi.org/10.1016/j.bbadva.2023.100091.
[56] A.S. Ladokhin, M.L. Malak Henryk, J.R. Lakowicz Johnson, L. Wang, A. W. Steggles, P.W. Holloway, Frequency-domain fluorescence of mutant cytochrome b5, in: Proceedings of SPIE -The International Society for Optical Engineering - Time-Resolved Laser Spectroscopy in Biochemstry III, The International Society for Optical Engineering, 1992, pp. 562–569.
[57] S. Vitiello, M. Caselli, G. Pavesi, M. Santucci, S. Ferrari, M. Paola Costi, G. Ponterini, Intrinsic fluorescence of the active and the inactive functional forms of human thymidylate synthase, ChemBioChem 22 (2021) 1800–1810, https://doi.org/10.1002/cbic.202000722.
[58] A. Micsonai, É. Bulyáki, J. Kardos, BeStSel: From secondary structure analysis to protein fold prediction by circular dichroism spectroscopy, in: Methods in Molecular Biology, Humana Press Inc., 2021, pp. 175–189, https://doi.org/10.1007/978-1-0716-0892-0_11.
[59] M. Meglioli, F. Sebastiani, M. Bellei, G. Di Rocco, A. Ranieri, C.A. Bortolotti, M. Sola, M. Borsari, G. Smulevich, G. Battistuzzi, Electrochemical and spectroscopic characterization of co-Neuroglobin: a Bioelectrocatalyst for H2 production, Inorg. Chem. (2025), https://doi.org/10.1021/acs.inorgchem.5c00551.
[60] H.A. Havel (Ed.), Spectroscopic Methods for Determining Protein Structure in Solution, VCH Publishers, New York, Weinheim, Cambridge, 1996.
[61] B.J. Reeder, D.A. Svistunenko, M.T. Wilson, Lipid binding to cytoglobin leads to a change in haem co-ordination: a role for cytoglobin in lipid signalling of oxidative stress, Biochem. J. 434 (2011) 483–492, https://doi.org/10.1042/BJ20101136.
[62] M.T. Wilson, B.J. Reeder, The peroxidatic activities of myoglobin and hemoglobin, their pathological consequences and possible medical interventions, Mol. Asp. Med. 84 (2022), https://doi.org/10.1016/j.mam.2021.101045.
[63] I. Al Ghouleh, N.K.H. Khoo, U.G. Knaus, K.K. Griendling, R.M. Touyz, V. J. Thannickal, A. Barchowsky, W.M. Nauseef, E.E. Kelley, P.M. Bauer, V. Darley-Usmar, S. Shiva, E. Cifuentes-Pagano, B.A. Freeman, M.T. Gladwin, P.J. Pagano, Oxidases and peroxidases in cardiovascular and lung disease: new concepts in reactive oxygen species signaling, Free Radic. Biol. Med. 51 (2011) 1271–1288, https://doi.org/10.1016/j.freeradbiomed.2011.06.011.
[64] H. Sies, Hydrogen peroxide as a central redox signaling molecule in physiological oxidative stress: oxidative eustress, Redox Biol. 11 (2017) 613–619, https://doi.org/10.1016/j.redox.2016.12.035.
[65] A. Kapralov, I.I. Vlasova, W. Feng, A. Maeda, K. Walson, V.A. Tyurin, Z. Huang, R. K. Aneja, J. Carcillo, H. Bayir, V.E. Kagan, Peroxidase activity of hemoglobin·haptoglobin complexes. Covalent aggreation and oxidative stress in plasma and macrophages, J. Biol. Chem. 284 (2009) 30395–30407, https://doi.org/10.1074/jbc.M109.045567.
[66] E. Singh, A. Gupta, P. Singh, M. Jain, J. Muthukumaran, R.P. Singh, A.K. Singh, Exploring mammalian heme peroxidases: a comprehensive review on the structure and function of myeloperoxidase, lactoperoxidase, eosinophil peroxidase, thyroid peroxidase and peroxidasin, Arch. Biochem. Biophys. 761 (2024), https://doi.org/10.1016/j.abb.2024.110155.
[67] B. Valeur, M.N. Berberan-Santos, Molecular Fluorescence, Wiley, 2012, https://doi.org/10.1002/9783527650002.
[68] P. Ascenzi, M. Marino, F. Polticelli, M. Coletta, M. Gioia, S. Marini, A. Pesce, M. Nardini, M. Bolognesi, B.J. Reeder, M.T. Wilson, Non-covalent and covalent modifications modulate the reactivity of monomeric mammalian globins, Biochim. Biophys. Acta, Proteins Proteomics 2013 (1834) 1750–1756, https://doi.org/10.1016/j.bbapap.2013.02.012.
[69] G. Smulevich, Understanding heme cavity structure of peroxidases: comparison of electronic absorption and resonance raman spectra with crystallographic results, Biospectroscopy 4 (1998) S1–S17, https://doi.org/10.1002/(SICI)1520-6343(1998)4:5+%3CS3::AID-BSPY2%3E3.0.CO;2-R.
[70] G. Smulevich, M. Paoli, G. De Sanctis, A.R. Mantini, F. Ascoli, M. Coletta, Spectroscopic evidence for a conformational transition in horseradish peroxidase at very low pH, Biochemistry 36 (1997) 640–649, https://doi.org/10.1021/bi960427b.
[71] M.W. Makinen, A.K. Churg, Structural andbanalytical aspects of the electronic spectra of hemeproteins, in: A.B.P. Lever, H.B. Gray (Eds.), Iron Porphyrins, Addison-Wesley, London-Amsterdam, 1983, pp. 141–235.
[72] F. Neri, D. Kok, M.A. Miller, G. Smulevich, Fluoride binding in hemoproteins: the importance of the distal cavity structure, Biochemistry 36 (1997) 8947–8953, https://doi.org/10.1021/bi970248+.
[73] G.R. Moore, G.W. Pettigrew, Cytochromes c. Evolutionary, Structural and Physicochemical Aspects, Springer, Berlin Heidelberg, Berlin, Heidelberg, 1990, https://doi.org/10.1007/978-3-642-74536-2.
[74] G. De Simone, P. Fattibene, F. Sebastiani, G. Smulevich, M. Coletta, P. Ascenzi, Dissociation of the proximal his-Fe bond upon NO binding to ferrous zebrafish nitrobindin, J. Inorg. Biochem. 236 (2022), https://doi.org/10.1016/j.jinorgbio.2022.111962.
[75] M.P. Horvath, R.A. Copeland, M.W. Makinen, The second derivative electronic absorption spectrum of cytochrome c oxidase in the Soret region, Biophys. J. 77 (1999) 1694–1711, https://doi.org/10.1016/S0006-3495(99)77016-5.
[76] D. Sherman, S. Kotake, N. Ishibe, R.A. Copeland, Resolution of the electronic transitions of cytochrome c oxidase: evidence for two conformational states of ferrous cytochrome a, Proc. Natl. Acad. Sci. USA 88 (1991) 4265–4269, https://doi.org/10.1073/pnas.88.10.4265.
[77] I. Dragomir, A. Hagarman, C. Wallace, R. Schweitzer-Stenner, Optical band splitting and electronic perturbations of the heme chromophore in cytochrome c at room temperature probed by visible electronic circular dichroism spectroscopy, Biophys. J. 92 (2007) 989–998, https://doi.org/10.1529/biophysj.106.095976.
[78] R. Schweitzer-Stenner, D. Bigman, Electronic and vibronic contributions to the band splitting in optical spectra of heme proteins, J. Phys. Chem. B 105 (2001) 7064–7073, https://doi.org/10.1021/jp010703i.
[79] R. Schweitzer-Stenner, Heme–Protein Interactions and Functional Relevant Heme Deformations: The Cytochrome c Case, Molecules 27 (2022), https://doi.org/10.3390/molecules27248751.
[80] B. Vallone, K. Nienhaus, A. Matthes, M. Brunori, G.U. Nienhaus, The structure of carbonmonoxy neuroglobin reveals a heme-sliding mechanism for control of ligand affinity, Proc. Natl. Acad. Sci. 101 (2004) 17351–17356, https://doi.org/10.1073/pnas.0407633101.
[81] C. Exertier, F. Sebastiani, I. Freda, E. Gugole, G. Cerutti, G. Parisi, L. C. Montemiglio, M. Becucci, C. Viappiani, S. Bruno, C. Savino, C. Zamparelli, M. Anselmi, S. Abbruzzetti, G. Smulevich, B. Vallone, Probing the role of murine Neuroglobin CDloop-D-Helix unit in CO ligand binding and structural dynamics, ACS Chem. Biol. 17 (2022) 2099–2108, https://doi.org/10.1021/acschembio.2c00172.
[82] T. Uno, D. Ryu, H. Tsutsumi, Y. Tomisugi, Y. Ishikawa, A.J. Wilkinson, H. Sato, T. Hayashi, Residues in the distal heme pocket of neuroglobin: implications for the multiple ligand binding steps, J. Biol. Chem. 279 (2004) 5886–5893, https://doi.org/10.1074/jbc.M311748200.
[83] K. Nienhaus, J.M. Kriegl, G.U. Nienhaus, Structural dynamics in the active site of murine Neuroglobin and its effects on ligand binding, J. Biol. Chem. 279 (2004) 22944–22952, https://doi.org/10.1074/jbc.M401561200.
[84] A. Boffi, T.K. Das, S. Della Longa, C. Spagnuolo, D.L. Rousseau, Pentacoordinate hemin derivatives in sodium dodecyl sulfate micelles: model systems for the assignment of the fifth ligand in ferric heme proteins, Biophys. J. 77 (1999) 1143–1149, https://doi.org/10.1016/S0006-3495(99)76965-1.
[85] A.E. Pond, M.P. Roach, M. Sono, A.H. Rux, S. Franzen, R. Hu, M.R. Thomas, A. Wilks, Y. Dou, M. Ikeda-Saito, P.R. Ortiz De Montellano, W.H. Woodruff, S. G. Boxer, J.H. Dawson, Assignment of the heme axial ligand(s) for the ferric myoglobin (H93G) and heme oxygenase (H25A) cavity mutants as oxygen donors using magnetic circular dichroism, Biochemistry 38 (1999) 7601–7608, https://doi.org/10.1021/bi9825448.
[86] J. Du, M. Sono, J.H. Dawson, The H93G myoglobin cavity mutant as a versatile scaffold for modeling heme iron coordination structures in protein active sites and their characterization with magnetic circular dichroism spectroscopy, Coord. Chem. Rev. 255 (2011) 700–716, https://doi.org/10.1016/j.ccr.2011.01.029.
[87] H.X. Liu, L. Li, X.Z. Yang, C.W. Wei, H.M. Cheng, S.Q. Gao, G.B. Wen, Y.W. Lin, Enhancement of protein stability by an additional disulfide bond designed in human neuroglobin, RSC Adv. 9 (2019) 4172–4179, https://doi.org/10.1039/c8ra10390a.
[88] H. Ji, Y. Guo, H. Li, T. Xu, L. Li, Fluorescence spectra of human neuroglobin, Spectrosc. Lett. 51 (2018) 17–21, https://doi.org/10.1080/00387010.2017.1405992.
[89] L. Huang, L. Li, H. Li, S. Tian, H. Cui, J. Kong, Interaction between Neuroglobin and caffeine by multispectroscopic methods, Spectrosc. Lett. 46 (2013) 433–440, https://doi.org/10.1080/00387010.2012.753091.
[90] Z. Gryczynski, T. Tenenholz, E. Bucci, Rates of energy transfer between tryptophans and hemes in hemoglobin, assuming that the heme is a planar oscillator, Biophys. J. 63 (1992) 648–653, https://doi.org/10.1016/S0006-3495(92)81657-0.
[91] R.E. Hirsch, M.J. Lin, G.V.A. Vidugirus, S. Huang, J.M. Friedman, R.L. Nagel, Conformational changes in oxyhemoglobin C (Gluβ6 → Lys) detected by spectroscopic probing, J. Biol. Chem. 271 (1996) 372–375, https://doi.org/10.1074/jbc.271.1.372.

[92] S. Verheyden, A. Sillen, A. Gils, P.J. Declerck, Y. Engelborghs, Tryptophan properties in fluorescence and functional stability of plasminogen activator inhibitor 1, Biophys. J. 85 (2003) 501–510, https://doi.org/10.1016/S0006-3495(03)74495-6.
[93] M. Khrenova, I. Topol, J. Collins, A. Nemukhin, Estimating orientation factors in the FRET theory of fluorescent proteins: the TagRFP-KFP pair and beyond, Biophys. J. 108 (2015) 126–132, https://doi.org/10.1016/j.bpj.2014.11.1859.
[94] A.G. Szabo, D. Kpajcarski, M. Zuker, B. Alpert, Conformational heterogeneity in hemoglobin as determined by picosecond fluorescence decay measurements of the tryptopran residues, Chem. Phys. Lett. 108 (1984) 145–149, https://doi.org/10.1016/0009-2614(84)85709-7.
[95] Y. Engelborghs, The analysis of time resolved protein fluorescence in multi-tryptophan proteins, Spectrochim. Acta A Mol. Biomol. Spectrosc. 57 (2001) 2255–2270, https://doi.org/10.1016/S1386-1425(01)00485-1.
[96] E. Bucci, H. Malak, C. Fronticelli, I. Gryczynski, J.R. Lakowicz, Resolution of the lifetimes and correlation times of the intrinsic tryptophan fluorescence of human hemoglobin solutions using 2 GHz frequency-domain fluorometry, J. Biol. Chem. 263 (1988) 6972–6977, https://doi.org/10.1016/S0021-9258(18)68591-6.
[97] B.S. Perrin, T. Ichiye, Identifying residues that cause pH-dependent reduction potentials, Biochemistry 52 (2013) 3022–3024, https://doi.org/10.1021/bi4002858.
[98] T. Brittain, The anti-apoptotic role of neuroglobin, Cells 1 (2012) 1133–1155, https://doi.org/10.3390/cells1041133.
[99] K. Jin, X.O. Mao, L. Xie, A.A. Khan, D.A. Greenberg, Neuroglobin protects against nitric oxide toxicity, Neurosci. Lett. 430 (2008) 135–137, https://doi.org/10.1016/j.neulet.2007.10.031.
[100] R.C. Li, M.W. Morris, S.K. Lee, F. Pouranfar, Y. Wang, D. Gozal, Neuroglobin protects PC12 cells against oxidative stress, Brain Res. 1190 (2008) 159–166, https://doi.org/10.1016/j.brainres.2007.11.022.
[101] S.N. Vinogradov, L. Moens, Diversity of globin function: enzymatic, transport, storage, and sensing, J. Biol. Chem. 283 (2008) 8773–8777, https://doi.org/10.1074/jbc.R700029200.
[102] E. Fordel, L. Thijs, L. Moens, S. Dewilde, Neuroglobin and cytoglobin expression in mice: evidence for a correlation with reactive oxygen species scavenging, FEBS J. 274 (2007) 1312–1317, https://doi.org/10.1111/j.1742-4658.2007.05679.x.
[103] J. Liu, Z. Yu, S. Guo, S.R. Lee, C. Xing, C. Zhang, Y. Gao, D.G. Nicholls, E.H. Lo, X. Wang, Effects of neuroglobin overexpression on mitochondrial function and oxidative stress following hypoxia/reoxygenation in cultured neurons, J. Neurosci. Res. 87 (2009) 164–170, https://doi.org/10.1002/jnr.21826.
[104] C. Mathai, F.L. Jourd'heuil, R.I. Lopez-Soler, D. Jourd'heuil, Emerging perspectives on cytoglobin, beyond NO dioxygenase and peroxidase, Redox Biol. 32 (2020), https://doi.org/10.1016/j.redox.2020.101468.
[105] D. Li, X.Q. Chen, W.J. Li, Y.H. Yang, J.Z. Wang, A.C.H. Yu, Cytoglobin up-regulated by hydrogen peroxide plays a protective role in oxidative stress, Neurochem. Res. 32 (2007) 1375–1380, https://doi.org/10.1007/s11064-007-9317-x.
[106] N. Kawada, D.B. Kristensen, K. Asahina, K. Nakatani, Y. Minamiyama, S. Seki, K. Yoshizato, Characterization of a stellate cell activation-associated protein (STAP) with peroxidase activity found in rat hepatic stellate cells, J. Biol. Chem. 276 (2001) 25318–25323, https://doi.org/10.1074/jbc.M102630200.
[107] N.J. Hodges, N. Innocent, S. Dhanda, M. Graham, Cellular protection from oxidative DNA damage by over-expression of the novel globin cytoglobin in vitro, Mutagenesis 23 (2008) 293–298, https://doi.org/10.1093/mutage/gen013.
[108] P. George, D.H. Irvine, Reaction of Metmyoglobin with hydrogen peroxide, Nature 168 (1951) 164–165, https://doi.org/10.1038/168164b0.
[109] E. Antonini, M. Brunori, Hemoglobin and Myoglobin in their Reactions with Ligands, North-Holland Pub. Co., Amsterdam, 1971.
[110] R.E.M. Diederix, M. Ubbink, G.W. Canters, Peroxidase activity as a tool for studying the folding of c-type cytochromes, Biochemistry 41 (2002) 13067–13077, https://doi.org/10.1021/bi0260841.
[111] R.E.M. Diederix, M. Ubbink, G.W. Canters, Effect of the protein matrix of cytochrome c in suppressing the inherent peroxidase activity of its heme prosthetic group, ChemBioChem 3 (2002) 110–112, https://doi.org/10.1002/1439-7633(20020104)3:1<110::AID-CBIC110>3.0.CO;2-2.
[112] S. Watanabe, N. Takahashi, H. Uchida, K. Wakasugi, Human neuroglobin functions as an oxidative stress-responsive sensor for neuroprotection, J. Biol. Chem. 287 (2012) 30128–30138, https://doi.org/10.1074/jbc.M112.373381.